catalysts

MDPI

Review

Supported Catalysts for CO_2 Methanation: A Review

Patrizia Frontera [1,2], Anastasia Macario [3,*], Marco Ferraro [4] and PierLuigi Antonucci [1]

1 Civil Engineering, Energy, Environmental and Materials Department, University Mediterranea of Reggio Calabria, 89134 Reggio Calabria, Italy; patrizia.frontera@unirc.it (P.F.); pierluigi.antonucci@unirc.it (P.A.)
2 Consorzio Interuniversitario per la Scienza e la Tecnologia dei Materiali—INSTM, 50121 Firenze, Italy
3 Environmental&Chemical Engineering Department, University of Calabria, 87036 Rende, Italy
4 Consiglio Nazionale delle Ricerche—Istituto di Tecnologie Avanzate per l'Energia "Nicola Giordano", IT-98126 Messina, Italy; marco.ferraro@itae.cnr.it
* Correspondence: macario@unical.it; Tel.: +39-0984-496-704

Academic Editors: Benoît Louis, Qiang Wang and Marcelo Maciel Pereira
Received: 16 December 2016; Accepted: 8 February 2017; Published: 13 February 2017

Abstract: CO_2 methanation is a well-known reaction that is of interest as a capture and storage (CCS) process and as a renewable energy storage system based on a power-to-gas conversion process by substitute or synthetic natural gas (SNG) production. Integrating water electrolysis and CO_2 methanation is a highly effective way to store energy produced by renewables sources. The conversion of electricity into methane takes place via two steps: hydrogen is produced by electrolysis and converted to methane by CO_2 methanation. The effectiveness and efficiency of power-to-gas plants strongly depend on the CO_2 methanation process. For this reason, research on CO_2 methanation has intensified over the last 10 years. The rise of active, selective, and stable catalysts is the core of the CO_2 methanation process. Novel, heterogeneous catalysts have been tested and tuned such that the CO_2 methanation process increases their productivity. The present work aims to give a critical overview of CO_2 methanation catalyst production and research carried out in the last 50 years. The fundamentals of reaction mechanism, catalyst deactivation, and catalyst promoters, as well as a discussion of current and future developments in CO_2 methanation, are also included.

Keywords: carbon dioxide; methane; metal catalysts; hydrogenation; power-to-gas

1. Introduction

Several studies [1–9] and recent reviews [10–14] have focused on the methanation reaction, mainly due to its important implications for energy and the environment. Methanation processes produce methane (*Substitute* or *Synthetic* Natural Gas, SNG) from hydrogen and CO_x. CO and CO_2 methanation processes, discovered in 1902 by Paul Sabatier and Jean-Baptiste Senderens, represent a promising solution for reducing anthropogenic gas emissions [11].

The increasing use of renewable sources, due to their fluctuating character, makes mandatory the development of adequate storage systems in order to overcome the mismatch between power production and instantaneous demand (Figure 1). Water electrolysis is a mature technology to produce hydrogen and CO_2 can be conveniently recovered from several industrial processes, such as biomass combustion and gasification, biogas facilities, power plants, oil refineries, and cement kilns.

The reaction is also considered a key technology able to facilitate future manned space missions by the recycling of CO_2 from breathing or wasted H_2 from water electrolysis on the International Space Station [15–17].

The methanation of CO_2 is an exothermic reaction (Equation (1)), typically operating between 200 °C and 450 °C, depending on the catalyst and experimental conditions [8,10]. Although several papers have been published on the subject in the recent past, no general consensus exists on the

reaction's operating mechanism, mainly due to the uncertainty in determining the intermediate compound involved in the rate determining step [10,11].

$$CO_2 + 4H_2 \leftrightarrow CH_4 + 2H_2O_{(g)} \quad \Delta H_{298K} = -164 \frac{kJ}{mol} \tag{1}$$

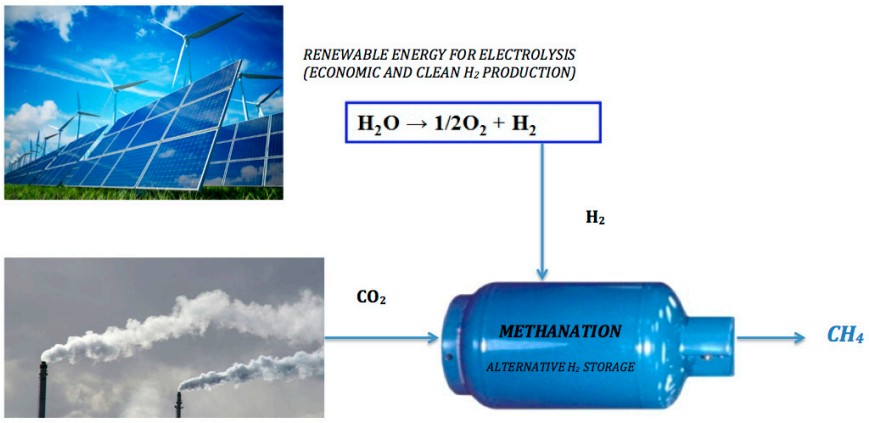

Figure 1. CO_2 methanation as an alternative to H_2 storage.

The first and most popular path considers the conversion of CO_2 to CO, which, in turn, is hydrogenated to CH_4 by the same mechanism involved in CO methanation. The second path includes the direct hydrogenation of CO_2 to CH_4, without formation of any CO intermediate (Figure 2). As said above, numerous reviews exist on this argument (i.e., mechanistic aspects, reactor type modeling, simulation); therefore, it is outside the scope of the present paper [10,11].

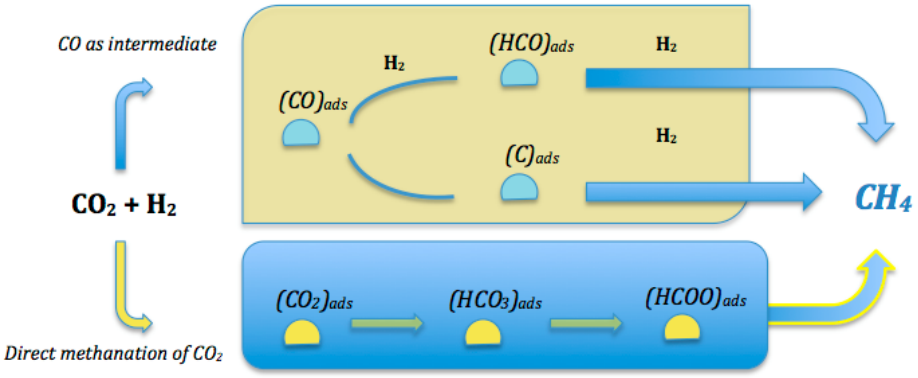

Figure 2. Simplified reaction mechanisms of CO_2 methanation.

The first part of the paper is dedicated to noble metal catalysts. These have so far demonstrated a high performance in the reaction, so are of relative interest from an industrial point of view on account of their high cost. Therefore, most of the discussion on the subject is devoted to Ni-based materials that couple a high catalytic activity and affordable cost.

Transition metals were deeply investigated as active catalysts for CO_2 hydrogenation [18–20], and affect the CO_2 activation and reduction steps. Iron, cobalt, nickel, and copper show high catalytic properties for CO_2 activation. Chemisorption of carbon dioxide on transition metals is spontaneous, while the surface structure of the metal strongly affects the thermodynamic of the catalytic process [18]. For example, the binding energy of carbon dioxide on the iron surface is stronger than that of platinum, while the CO_2 dissociation proceeds more easily on platinum than on iron [19]. All these works demonstrate that metal plays a pivotal role in CO_2 hydrogenation (both in the activation and reduction steps).

In order to preserve and improve metal activity, reduction technology focused on the metal-supported catalyst development [21]. The physico-chemical characteristics (structure, chemical composition, defect groups, and thermal stability) of supports are fundamental aspects to consider in metal-supported catalyst tuning because they affect the activity, productivity, and lifetime of the final heterogeneous catalyst. The interactions between support and metal were studied by different researchers in many reactions of environmental interest, such as dry reforming, steam reforming, partial oxidation, and autothermal reforming [22–29].

2. Catalytic Materials for CO_2 Methanation Reaction

This section provides a concise and precise description of the experimental results, their interpretation, and the experimental conclusions that can be drawn.

2.1. Noble Metal Catalysts

2.1.1. Rhodium

Rh is one of the most investigated metals for the CO_2 methanation reaction. Particular emphasis has so far been placed on the hypotheses of a mechanism that allows methane to be formed on the surface of the catalyst, especially in the presence of alumina as a support. The steps leading to methane could be: (i) chemisorption of carbon dioxide; (ii) dissociation of carbon dioxide into CO and O adsorbed on the surface; (iii) reaction of dissociated species with hydrogen [30]. The oxidation state of the metal may also play an important role in the evolution of the reaction, since CO_2 oxidizes the catalyst. Moreover, the production of methane depends upon the temperature, pressure, presence, and absence of promoters. Obviously, when varying the Rh content different metal particle sizes are formed, and at low temperatures (130–150 °C) the activity of larger particle sizes of Rh was found to be higher than that of smaller ones. Furthermore, the addition of Ba and K on the Al_2O_3 support allows significant differences in the catalytic behavior in the temperature range 300–700 °C. CH_4 was preferentially formed below 500 °C on Ba-containing and pure Rh/Al_2O_3 while, at higher temperatures, significant amounts of CO were formed. Only CO was observed with the K-containing catalyst [30–33].

The presence of O_2 could have a positive effect on the methanation of CO_2 and CO. Belus et al. highlighted that oxygen, in low proportion, improves the catalytic performance of the $Rh/\gamma\text{-}Al_2O_3$ catalyst, but if the amount of O_2 is too high, a negative effect is observed [31]. In Figure 3 the methane production, over $Rh(1\%)/\gamma\text{-}Al_2O_3$ catalyst, at 125 °C, as a function of CO/O_2 and CO_2/O_2 is reported. DRIFTS experiments explain that the positive effect of oxygen is due to the formation of more active species, such as gem-dicarbonyl. On the contrary, the negative effect could be attributed to the inevitable oxidation of the catalyst [31].

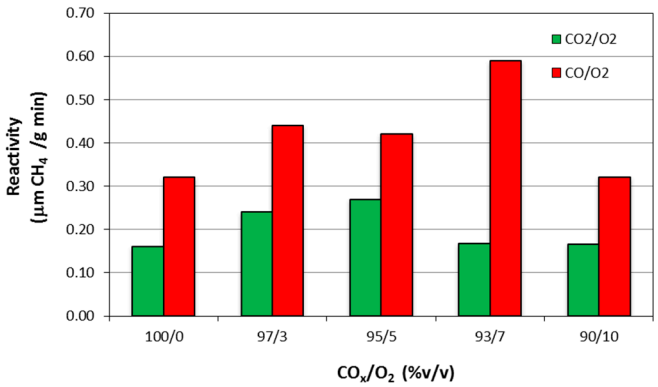

Figure 3. CH_4 production (µmol of methane by gram of catalyst/minute) as a function of CO_2/O_2 and CO/O_2 ratios, over $Rh(1\%)/\gamma\text{-}Al_2O_3$ catalyst, at 125 °C. Adapted from Beuls et al. [31].

A synergistic effect was recently observed by mechanically mixing Rh/γ–Al_2O_3 and Ni/activated carbon (Ni/AC). It appears that higher production of CH_4, with respect to the single catalysts, is not due to a chemical interaction since no formation of new structures occurs when the catalysts are mixed. Authors hypothesize that Rh/γ-Al_2O_3 is able to efficiently adsorb CO_2, whereas Ni/AC adsorbs a high amount of H_2 but a small amount of CO_2, resulting in high CO_2 conversion and methane formation [34].

TiO_2 has been also extensively investigated as a support for Rh in the CO_2 methanation reaction, especially at low temperatures. Rh/TiO_2 is one of the most active catalysts for the reaction, but the high cost of the metal prevents its widespread utilization at industrial scale. Such a high activity is thought to be attributed to a metal–support interaction that facilitates the breaking of the C=O bond, resulting in an increase of the catalytic activity [35–42]. Recently, the Density Functional Theory method (DFT) has been employed to study the CO_2 methanation reaction on an Rh_1/TiO_2 (101) model [43]. The results show the co-adsorption properties of the Rh_1/TiO_2 catalyst surface. By the proposed mechanism, CO_2 and H_2 are co-adsorbed on the Rh atom and, subsequently, can react with each other to form CO. Further adsorption of H_2 is inhibited on the CO adsorbed on Rh; therefore, the consecutive CO hydrogenation does not occur. The proposed mechanism explains why, experimentally, a high selectivity of Rh_1/TiO_2 to CO is observed, as a consequence of the frontier orbital charge density symmetry matching principle [44].

2.1.2. Ruthenium

Ru is one of the most active methanation catalysts. Its catalytic activity and selectivity to CH_4 are, however, largely dependent on the dispersion of the metallic phase (at high dispersion the apparent activation energy reaches a minimum), on the type of the support, and an addition of modifiers/promoters that can more or less chemically interact with the metal [45–54]. Ru catalysts have been supported on a number of oxide materials, such as Al_2O_3, TiO_2, SiO_2, MgO, $MgAl_2O_4$, C, and $Ce_{0.8}Zr_{0.2}O_2$ [55,56]. The activity of pre-reduced 3%Ru/Al_2O_3 catalyst (CO_2 conversion, CH_4 and CO yields), as a function of the reaction temperature, is reported in Figure 4 [53]. The best catalytic performance occurs at 673 K, with the highest CO_2 conversion, CH_4 yield, and limited CO yield.

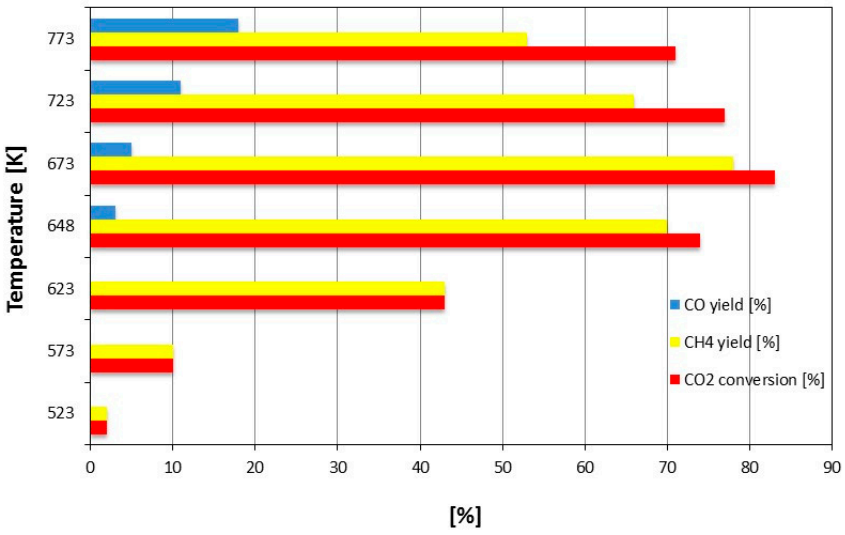

Figure 4. CO_2 conversion, CH_4 and CO yields on pre-reduced 3%Ru/Al_2O_3 catalyst and GHSV = 55000 h^{-1}, at different temperature reactions. Adapted from Garbarino et al. [53].

In particular, in order to lower the reaction temperature in CO_2 methanation reaction, Ru/TiO_2 catalysts have been used since the 1980s. Akamaru et al. [57] reported that they failed to reproduce the results of Gratzel et al. [58,59] using Ru/TiO_2 catalysts prepared under the same experimental conditions.

The main reason was the difficulty of controlling the preparation conditions in a wet process. Therefore, a dry technique, called polyhedral barrel sputtering, was developed; this technique, according to [60], is able to disperse metal nanoparticles on the support in clean conditions and control their size and deposition density. Using a Ru/TiO_2 catalyst prepared with this technique, an onset temperature of 60 °C for CH_4 generation was observed that increases upon increasing the size of metal particles. Recently, Xu et al. have demonstrated that the Ru particle size is not the main reason for the different behavior of Ru/rutile(TiO_2)catalyst [61]. They reported that the increasing of hydroxyl groups on the TiO_2 layer strongly increases the CO_2 dissociation. The suggested mechanism assumes that the adsorbed CO_2 reacts with the hydroxyl groups, producing CO via formate species intermediates. So, the pre-treatment temperature of the support should not be higher than 800 °C, because over this temperature value condensation of the hydroxyl groups occurs and the support does not play its important role.

Results of DFT analysis attribute the high activity of the catalyst to the difference between the Ru structure and the Ru surface, and to the weak charge transfer from adsorbed species to Ru atoms [57].

It is recognized that CeO_2 plays an important role in promoting CO_2 methanation and enhancing CH_4 formation. On account of its basicity, CO_2 is adsorbed on CeO_2 and reduced due to the oxygen vacancies on CeO_2, resulting in high CO_2 conversion at $T \leq 350$ °C. The addition of 30% CeO_2 to 2 wt % Ru/Al_2O_3 leads to an enlarged specific surface area of the catalyst. Furthermore, the reaction intermediates (formates, carbonates) react with H_2 faster on this catalyst than over Ru/Al_2O_3 [62]. Ceria is also a very good methanation catalyst when doped with 0.05 wt % Ru. Electron microscopy and XRD analyses suggest that Ru is incorporated into the ceria lattice. At T = 450 °C, this catalyst converts 55% CO_2 with 99% selectivity to CH_4. The reaction takes place on the reduced $Ce_{0.95}Ru_{0.05}O_2$; the role of Ru is to lower the reduction temperature with respect to pure ceria [63].

Ru supported on TiO_2–Al_2O_3 exhibits a much higher (3.1 times) activity than that on supported Al_2O_3. This result was attributed to the smaller averaged particle size of Ru supported on TiO_2–Al_2O_3 (2.8 nm) versus the 4.3 nm measured on Al_2O_3, resulting from the interaction between the metal and the rutile TiO_2, which hinders the aggregation of Ru particles [64].

Very recently, trimetallic catalysts drew attention to the reaction of the Baker group [65–67], which highlights how the adsorption strength of CO_2 is controlled by the Lewis basicity of the catalyst, the d-band center of the metal surface, and the charge transfer from the metal surface to the chemisorbed CO_2. Pd, Rh, and Ru supported on Mn/Cu–Ce–Al_2O_3 catalysts were also investigated and Ru/Mn/Cu–Al_2O_3 was found to be the most promising catalyst (10.9 wt % Ru loading, calcination temperature 1035 °C). Baker et al. claim the suitability of their catalysts for industrial application.

2.1.3. Palladium

A good catalytic performance has also been observed with Pd-based catalysts. Pd is able to dissociate molecular hydrogen [68,69] and makes available hydrogen atoms for the subsequent transfer and reaction with activated surface carbonate species formed by the reaction of CO_2 on a Mg-containing oxide [70–72],with the aim of providing a pathway to minimize CO formation by using metal oxides that inhibit CO desorption. Intermixed Pd and Mg sites are obtained by using the reverse microemulsion synthesis route; 95% selectivity to CH_4 and 59% CO_2 conversion have been measured at 450 °C [73].

More recently, shape-controlled Pd nanoparticles embedded in mesoporous silica have been tested in the reaction; their performance has been compared with a Pd/SiO_2 catalyst prepared by wet impregnation. The encapsulation was demonstrated to have a better stability towards sintering. Moreover, different activities and selectivities for the CO_2 methanation were demonstrated by the different exposed facets (100, 111) of the metal [74].

2.2. Nickel-Based Catalysts

Supported Ni catalysts are the most widely investigated materials for CO_2 methanation due to their high efficiency in CH_4 production and low cost [75–89]. A lot of supports have been investigated

for Ni catalysts since, as is well known, the catalytic performance strongly depends upon the nature and properties of the support. Its influence can be generally linked to physico-chemical peculiarities: (i) varying the dispersion of the active phase; (ii) modifying the reducibility of the oxide precursors by tuning the interaction between the active phase and the support.

In this part of the review, we will examine the role of the most investigated supports for the hydrogen reaction with CO_2 to CH_4 (Al_2O_3, zeolites, SiO_2, CeO_2, ZrO_2, and Ce–ZrO_2) with particular emphasis on the role of promoters/modifiers in their catalytic performance in the reaction. Other materials were recently investigated as nickel supports, such as hydrotalcite, carbon nanotubes, and W–Mg oxides. Sections 2.2.4 and 2.2.5 will be dedicated to the main outcomes reached using these unconventional supports.

2.2.1. Alumina-Supported Nickel

The Ni/Al_2O_3 catalyst shows a high catalytic activity, although it suffers from severe carbon deposition or poor stability due to the high reaction temperature used [88,90]. Therefore, the aim throughout the years was to develop catalysts able to show both high activity and resistance to carbonaceous deposits in the reaction. So, since the pioneering work of Trimm et al. [91], a lot of papers have been published on the argument. We will examine here only the most recent ones, since the number of studies covering the topic is huge, and other previous reviews can easily be found in the literature. Rahamani et al. [92] have prepared, by impregnation, a series of Ni catalysts supported on mesoporous nanocrystalline γ-Al_2O_3, having high surface area and different Ni contents. The influence of calcination temperature was also investigated on CO_2 conversion and CH_4 selectivity. The catalyst with 20 wt % Ni shows higher activity and stability between 200 °C and 350 °C. According to He et al. [89], the combination of highly dispersed Ni particles with a strong basic support is thought to be responsible for the high performance of the Ni–Al hydrotalcite-derived catalyst. Such basic sites are originated from the formation of the Ni–O–Al structure; 100% CH_4 selectivity and 82% CO_2 conversion are reached at 350 °C.

In [93] a study on the methane yield as a function of different Ni-based compositions and reaction temperatures (250–500 °C) is reported. The data suggest that good performance is obtained at the expense of a CO intermediate on the corners of nanoparticles interacting with alumina, likely via an oxygenate mechanism.

In the light of a fluctuating supply of renewable hydrogen, various IR studies, under both stationary and transient conditions, have been done in order to get insight into the reaction mechanism. Since Ni is very prone to oxidation, studies have been carried out under "*operando*" conditions [94–98].

The results reported in [94] (81% CO_2 conversion, 80% CH_4 yield at 400 °C with a 23 wt % of $Ni/CaO/Al_2O_3$ catalyst), however, strongly suggest the importance of conducting experiments under realistic (i.e., transient) conditions. To ameliorate the performance of Ni/Al_2O_3 catalysts via substantial modifications of some specific (structural, electronic) properties, the addition of several promoters has been also attempted. Among these, CeO_2 has often been employed on account of some positive effects, such as: (i) improvement of the thermal stability of Al_2O_3; (ii) promotion of the dispersion of the metal onto the support; (iii) change of the properties of the metal due to strong metal–support interaction (SMSI) [41,89,99–101].

Moreover, CeO_2 is a well-known oxygen storage material, able to store and release in a reversible manner large amounts of oxygen depending on the experimental conditions adopted [102]. The results show that the presence of CeO_2 has significant influence on CO_2 conversion (for Ni/Al_2O_3, from 350 °C to 400 °C, 45% vs. 71% with a CeO_2 content of 2 wt %). CH_4 selectivity, independently from the CeO_2 content, is higher than 99%. Stability was measured for a reaction time up to 120 h [103]. In [104], the effect of different promoters (CeO_2, MnO_2, IrO_2, La_2O_3) on the catalytic performance of Ni supported on Al_2O_3 mesoporous nanoparticles was investigated. Both CO_2 conversion and CH_4 selectivity were demonstrated to be affected by the different promoters. The catalyst promoted by

ceria exhibits the highest activity; also in this case, the catalyst with 2 wt % ceria was the most active and selective to CH_4. The best results were obtained at 350 °C.

Few works have been published on Ni supported on zeolites for CO_2 methanation [49,105–107]. Recently, Graca et al. [108] prepared, by ion exchange and impregnation, Ni–Ce catalysts supported on a partially exchanged HNaUSY zeolite.

Since temperatures >800 °C are necessary to reduce the exchanged Ni species, those present on the catalyst prepared by Graca et al. [108] are not in the metal form during the reaction; the activity observed was attributed to the zeolite support. Moreover, addition of ceria causes an improvement in both CO_2 conversion and CH_4 selectivity [41,108–110]. Thus, the catalyst properties result from the synergistic effect between the metal active sites and the promoters. The "*operando*" IR spectroscopy technique was also used to get a better insight into the mechanism of the reaction. According to [111], dissociated hydrogen reacts with carbonates and/or physisorbed CO_2, giving rise firstly to formation of monodentate formates, then carbonyls, and finally to CH_4.

Recently, Rivero-Mendoza et al. reported La–Ni/γ-Al_2O_3 catalytic activity relative to the Sabatier reaction [112], where catalytic studies coupled with in situ DRIFTS analyses provide insights on the CO_2 methanation mechanism. The activation process of the catalyst promotes formation of oxidized Ni particles (Ni^{2+}) decorated with LaO_x moieties. During the reaction, in situ reduction of Ni occurs and LaO_x species return to their initial oxidation state (La_2O_3). Since the in situ DRIFTS analyses results show the presence of adsorbed formates and CO species, it is reasonable to think that the Sabatier reaction, catalyzed by the La–Ni/γ-Al_2O_3 catalyst, advances by the CO-based mechanism.

2.2.2. Silica-Supported Nickel

Metal–support interactions are generally present, although at a variable extent in t heterogeneous catalytic systems, implying that different combinations result in different performances in terms of activity and selectivity for a given process [113–115]. Among the numerous SiO_2-based materials used as supports for metal catalysts, mesostructured silica nanoparticles (MSN) have recently found wide application in several processes and reactions, such as in drug delivery [116,117], biomedical imaging [118,119], and catalysis [120,121]. Their unique features include (i) nanosized dimension; (ii) ordered structures; (iii) very high surface area; (iv) large pore volume; (v) tunable pore size from 1.5 to 10 nm; (vi) tailorable pore diameters to host particles of different dimensions [122].

Recently, Aziz et al. have studied such materials, promoted by Ni, for CO_2 methanation [123–125]. In [126] MSN (mesostructured silica nanoparticles) and Ni/MSN were prepared by sol-gel and impregnation methods. The reaction was carried out at temperatures between 150 °C and 450 °C. Ni/MSN was compared with other types of support; the activity of the reaction follows the order Ni/MSN > Ni/MCM-41 > Ni/HY > Ni/SiO_2 > Ni/γ-Al_2O_3. IR characterization supports the hypothesis that the high activity of Ni/MSN is due to the high concentration of basic sites on account of the presence of both intra- and inter-particle porosity. The carbon species detected on the surface was attributed to the presence of defect sites and/or oxygen vacancies in MSN. The role of Ni sites is that of dissociating H_2 to form atomic hydrogen, which, by reacting with the surface carbon species, forms CH_4. A 200-h endurance test shows no deactivation for the Ni/MSN catalyst.

In [124], various metals were loaded on MSNs (Rh, Ru, Ni, Fe, Ir, Cu, Zn, V, Cr, Mn, Al, and Zr). The catalytic performance measurements clearly indicate that surface centers containing metallic and associated basic and/or oxygen vacancy sites are responsible for the catalytic activity. This latter, at 350 °C, follows the order Rh/MSN > Ru/MSN > Ni/MSN > Ir/MSN > Fe/MSN > Cu/MSN. However, on an areal basis, Ni/MSN exhibits the best performance. In the light of the catalytic activity tests and physico-chemical characterization results, a new, plausible pathway in the mechanism of CO_2 methanation on metal based MSNs is formulated [12,124]. Firstly, CO_2 and H_2 are adsorbed on metal sites, and subsequently dissociate to form CO, O, and H atoms and migrate on the MSN surface. CO interacts with the oxides of MSN and forms bridged and linear carbonyls. Bidentate formate is also formed by interaction with atomic hydrogen. At the same time, the O atom splits onto the MSN surface

and is stabilized in the oxygen vacancy near the metal site. Hydroxyls are formed on the MSN surface by interaction of adsorbed oxygen with atomic hydrogen, and, by reaction with another hydrogen atom, water is formed [12,124]. Then, the carbon species is hydrogenated to CH_4. According to the Aziz et al., linear and bridged carbonyl, as well as bidentate formate, could be intermediates during the reaction course, as previously suggested [127–131].

In short, the role of MSN is the seat of sites for carbonyl species that are precursors for methane formation. In [125] the effect of Ni loading and water vapor on the performance and properties of Ni/MSN for CO_2 methanation was investigated. It is well known that metal loading on a supported catalyst significantly affects its dispersion and interaction with the support, in turn affecting the catalytic behavior. In general, the lower the metal loading, the higher its dispersion, and vice versa. In this study, results show that after increasing Ni loading from 1 to 10 wt %, a decrease in crystallinity, surface area, and basicity of the catalysts is observed. On the other hand, the catalytic activity follows the order 10%Ni/MSN ≈ 5Ni/MSN > 3Ni/MSN > 1Ni/MSN at 400 °C with 100% CO_2 conversion. It is then necessary to find a proper balance between Ni loading and basic sites concentration to achieve a high catalytic activity. As for the influence of water vapor on the feed stream, its presence was found to decrease the carbonyl species concentration on the surface of Ni/MSN, thus negatively affecting the catalytic activity of the reaction. It was suggested that such a negative effect could be attributed to the formation of CO_2 through the water gas shift (WGS) reaction between intermediate CO and excess water. Moreover, Ni sintering is favored by the presence of water vapor [132]. Finally, the optimal conditions for the reaction over Ni/MSN were singled out by response surface methodology (RSM). Accordingly, 85% CO_2 conversion could be achieved at 341 °C, 69.105 $mL_{cat} \cdot g^{-1} \cdot h^{-1}$ gas hourly space velocity (GHSV), and 3.68 H_2/CO_2 ratio.

Amorphous pure silica materials, well known as mesoporous materials, such as highly ordered hexagonal structure MCM-41, or large pore size and high specific surface area SBA-15 material, are typical supports largely studied by the scientific community for different catalytic applications.

However, few scientific papers have been published on the performance of Ni-incorporated MCM-41 catalysts in the methanation reaction.

In 2007, Du et al. employed C16Ni/MCM-41 catalysts (with C16 indicating a 16 carbon alkyl template producing MCM-41 pores with 2.9 nm diameter) with different amounts of incorporated Ni to be tested for CO_2 methanation [126]. A 3 wt % Ni catalyst at T = 300 °C shows 100% methane selectivity, although a very low CO_2 conversion (about 10% max) is observed. In our opinion, the main drawback of this type of support is due to its limited stability in the presence of steam. Since water is one of the products of methanation reactions, these supports should be useful only for catalyst activity at very low temperatures.

Very recently, Xin et al., from the Chemical Engineering School of Shanghai, studied mesoporous materials as a support for nickel catalysts and their application in CO methanation [7,133]. Both catalysts tested by Xin and co-workers—Ni-SBA-15, prepared by a traditional impregnation method [7], and Ni-MCM-41, synthesized by a hydrothermal synthesis method [133]—show promising behavior in CO methanation.

Methanation of producer gas (CO, H_2, CO_2, and other trace species [134,135] was also recently investigated on NiO/SBA-15 [136–139]. Firstly, CO_2 conversion increases on increasing the H_2/CO_2 ratio, up to a value of 6, and the maximum CO_2 conversion increases on increasing the NiO loading regardless of the preparation method (heat treatment (HT) or solvent impregnation (SI)) [140]. However, on using the HT method the NiO particles are preferentially dispersed outside the SBA-15 pores, whereas by the SI method they are included into the SBA-15 pores. As expected, the maximum CO_2 conversion and CH_4 yield, regardless of the preparation method, are obtained on increasing the NiO loading.

2.2.3. Zirconia- and Ceria-Supported Catalysts

The interest in ZrO_2 as a support for catalysts to be used in CO_2 methanation is mainly due to its acidic/basic characteristics and CO/CO_2 adsorption capability [141–143]. ZrO_2 exists in three polymorphic structures (monoclinic (m), tetragonal (t), and cubic (c)). The monoclinic phase is thermodynamically the most stable below 1000 °C; the other phases are stabilized at such lower temperatures by doping the solid phase with low valent cations. Polymorphs of ZrO_2 greatly influence their catalytic properties. For CO_2 methanation, Ni/t-ZrO_2 prepared from amorphous Ni–Zr alloys exhibits very high activity and almost 100% selectivity to methane at 200–300 °C [144,145]. It has been demonstrated that the catalytic activity increases with the amount of t-ZrO_2 [144,146], achieving the maximum methanation rate at 300 °C with a catalyst prepared from amorphous alloy precursors. The catalytic activity can be significantly enhanced on Ni/ZrO_2 catalysts prepared by Ni/Zr/earth elements alloys [147–150]. In the Ni/Zr/5at%Sm, samarium stabilizes tetragonal zirconia and increases the number of surface nickel atoms [146].

More recently, a highly efficient Ni/ZrO_2 catalyst doped with Yb_2O_3 for co-methanation of CO and CO_2 was developed. Over Ni6Zr2Yb at 300 °C, total conversion of CO and CO_2 was observed. More interestingly, a heat resistance test shows that, after 24 h of reaction at 800 °C, followed by going down to 300 °C, the conversion does not change the 89% value. Characterization results demonstrate that both activity and thermal stability are due to the formation of a (Zr-Yb) oxide having the cubic ZrO_2 structure. The promoting action of Yb_2O_3 was associated with the high solubility of Yb_2O_3 in the ZrO_2 lattice (the ionic radius of Yb^{+3}, 0.087 nm, is close to that of Zr^{+4}, 0.079 nm) [149].

Moreover, a 50% at%Ni–50%at(Zr-Sm oxide) with Zr/Sm = 5 calcined at 650 °C or 800 °C shows high activity for CO_2 methanation. The increase in Sm^{+3} ion content in the ZrO_2 lattice on increasing the calcination temperature leads to an increase in oxygen vacancies. According to the study of CO and CO_2 adsorption on tetragonal and monoclinic ZrO_2, the CO_2 adsorption capacity of m-ZrO_2 is more than one order of magnitude higher than that of t-ZrO_2, and the CO adsorption capacity of m-ZrO_2 is from 5 to 10 times higher than of t-ZrO_2 depending on the adsorption temperature [142]. As a consequence, the rate-determining step for the reaction cannot be the adsorption of CO_2 and CO. In this study, the high activity of Ni/t-ZrO_2 derives from the presence of oxygen vacancies, which allow a strong interaction with oxygen and weaken the C–O bond strength, leading to the enhancement of hydrogenation of CO_2 to CH_4 [150].

The most investigated rare-earth oxide as promoter of Ni–ZrO_2 catalysts for CO_2 methanation was ceria. Ceria was also studied as a single support for efficient Ni catalysts in CO_2 methanation [81,151–154], although its synergic effect with zirconia seems to increase the nickel performance.

The main role of ceria is attributed to its high oxygen storage capacity and ability to highly disperse nickel [155–159]. The Ce/Zr composition is a factor that has a strong influence on the catalytic performance of ceria-zirconia (CZ) in several types of reactions such as the reduction in three-way catalysts [160], the methane partial oxidation, and ethanol/methane reforming [161–163].

In [159] the C/Z composition of the mixed oxides fixes the ratio between the Ni^{2+} incorporated into the CZ fluorite structure and the surface Ni^0. Ni^{2+} enhances the catalyst specific activity; thus, a compromise between the two nickel species has to be found in order to optimize the catalytic system. Accordingly, a C/Z mass ratio of 60/40 leads to the best Ni^{2+}/Ni^0 ratio, resulting in the best catalytic activity. The mechanism of the reaction was also studied by Ocampo et al. on Ni/CZ under stoichiometric conditions [155,164]. The CO_2 conversion was observed to increase from 250 °C to 400 °C towards the thermodynamic value. Mono- and bidentate carbonates are present already at 150 °C, as detected by FTIR analysis. Thus, from the evidence shown in the work, the main reaction pathway does not involve CO as an intermediate. CO_2 adsorbs on the sites of mild basicity to form covalent carbonates, hydrogen carbonates, and then bidentate carbonates. These species are reduced and hydrogenated by H atoms formed by the dissociation of hydrogen on the surface of Ni^0 particles to form formates and finally release CH_4. However, a parallel pathway is hypothesized involving CO formed by a redox cycle on reduced ceria.

Pan et al. hold the presence of medium basic sites responsible for the high activity of Ni/CZ with respect to Ni/SiO_2 [165]. The equilibrium CO_2 conversion is reached at 340 °C. CO_2–TPD profiles of Ni/CZ show weak and medium sites, different from Ni/Al_2O_3, which shows weak and strong basic sites; CO_2 adsorbed on strong basic sites cannot desorb from Ni/Al_2O_3 surface until 700 °C. Consequently, the strongly adsorbed CO_2 on the surface does not participate in the reaction carried out from 220 °C to 400 °C. According to [166], CO_2 reacts with surface hydroxyls and surface oxygen to form hydrogen and monodentate carbonate, respectively [164,166–172]. Formate species could be also important intermediates during the reaction [63,173,174]. Combining CO_2–TPD and FTIR results, medium basic sites promote formation of monodentate formate and its hydrogenation during the CO_2 methanation, in accordance with [165,175]. The tetragonal phases, thought to be responsible for the activity in CZ-supported Ni catalysts, are distinguished into t, t', and t'', according to the type of tetragonal distortion and its nature. The t phase is a stable one and is formed through a diffusional phase decomposition; t' is obtained through a diffusionless transition and is metastable. The t'' form is intermediate between t' and cubic [176–179].

The H_2–TPR profiles reported in [180] show peaks in the temperature range from 400 °C to 600 °C for CZ, attributed to a reduction of surface oxygen and bulk oxygen in $Ce_{0.5}Zr_{0.5}O_2$, respectively [42,181,182], while the peaks around 360 °C are assigned to the reduction of surface oxygen in CZ and of the bulk NiO, having weak interaction with the support. Peaks at 400–600 °C are related to bulk oxygen in CZ and NiO having strong interaction with the support, or Ni ions incorporated into CZ [183]. In Figure 5 the qualitative behavior of TPR profiles (the data from our research are not yet published) of nickel catalysts supported on doped ceria with increasing nickel content is reported.

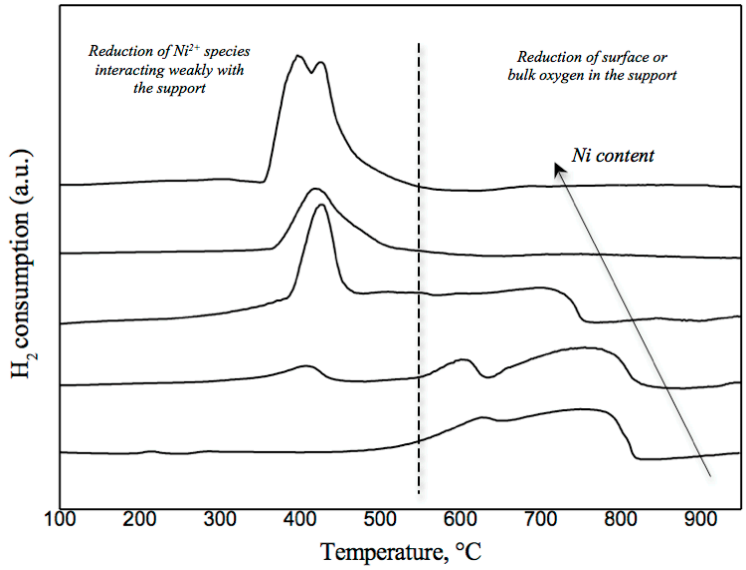

Figure 5. Qualitative TPR-H_2 profiles for impregnated Ni- supported on doped ceria.

Takano et al. recently investigated a 50 wt % Ni/(Zr + Ca) catalyst (molar ratios 0.125–0.333) affording 100% CH_4 selectivity with a CO_2 conversion of 90% at T = 400 °C. The comparison with 50 wt % Ni/(Zr + Sm) catalyst highlighted the higher conversion under the same flow rate conditions. The Ca content dependence of the catalytic activity has been related, according to [184], to the number of oxygen vacancies in t-ZrO_2 since calcium is a more effective additive than samarium. Hydrogen is atomically absorbed on Ni, and is able to reduce carbonates to formate, formaldehyde, methoxy species, and methane.

Other relevant papers on supported ZrO_2 and ceria Ni catalysts that must be cited for their significant results are [185–187]; moreover, an interesting paper regarding unconventional supports for

nickel catalysts has been published recently by Abate et al. [188]. This is a pioneering research work in which quaternary system catalysts have been prepared. In particular, the authors prepared a Ni-based catalyst by wet impregnation technique applied to γ-Al_2O_3 powder as a host for ZrO_2, TiO_2, and CeO_2 oxides. The best catalyst, named Ni/C15, is composed of a quaternary system with 55% γ-Al_2O_3 and 15% of each of the other oxides. The catalytic performance of the Ni/C15 catalyst in CO_2 methanation is superior to that of similar catalysts prepared with lower amounts of quaternary oxides (Ni/C5 and Ni/C10) and to that of nickel supported on commercial γ-Al_2O_3. A larger amount of all four oxides seems to favor the formation of large-sized nickel particles that are more active at lower temperatures. At 300 °C the CO_2 conversion to CH_4 is higher than 80%.

2.2.4. Hydrotalcite-Supported Nickel

With respect to the aforementioned conventional supports, other materials are emerging as potential, and sometime promising, supports for nickel catalyst in CO_2 methanation. Among these, the *hydrotalcite-like* compounds are noteworthy.

Hydrotalcite-like compounds, also known as layered double hydroxides, are layered structure materials composed of a mixed hydroxide of divalent/trivalent metals. The general representative chemical formula is $[M_{1-x}{}^{2+}M_x{}^{3+}(OH)_2](A^{n-})_{x/n}\bullet y\ H_2O$, where M^{2+} and M^{3+} are any divalent and trivalent cations, A^{n-} is an exchangeable interlayer anion (organic or inorganic), and the water molecules are either crystalline in the lattice or physisorbed on the surface [189].

Several authors have studied these materials as supports for Ni catalysts (Ni–Al/hydrotalcite), comparing their catalytic activity in CO_2 methanation with commercial Ni/γ-Al_2O_3 catalysts. Taking together the Abate et al. [190] and He et al. [191] results, it is possible to display the activity of Ni–Al/hydrotalcite catalysts prepared at three different pH values (12, 10, and 8.7). Both works report a high Ni dispersion on the hydrotalcite support with respect to the conventional catalyst (Ni/γ-Al_2O_3), indicating that this new support is a promising material for preparing stable and well-dispersed Ni catalysts. Even if the amount of loaded nickel on the support ranges between 75 and 80 wt %, the authors demonstrated that the catalysts possess a narrow nickel particle size distribution in the range of 3–9 nm. This means that more reducible nickel species can be obtained. The catalytic performance of Ni–Al–Hydrotalcite catalysts shows a maximum activity at 300 °C, with similar CO_2 conversion and CH_4 yield (85% for catalysts prepared by Abate et al. and 80%–82% for the catalyst prepared by He et al.).

Aluminum is the main metal present in this type of material; therefore, many works on the argument report the effect of the Ni/Al ratio on the catalyst performance. Gabrovska et al. [192] studied the variation of Ni^{2+}/Al^{3+} molar ratio effect on the catalytic activity of Ni-Al-Hydrotalcite. The effect on the catalyst performance cannot be defined directly but has to be correlated to other fundamental parameters of the CO_2 methanation process, such as reaction temperature, space velocity, and reduction temperature. The catalyst with the highest amount of Ni (Ni^{2+}/Al^{3+} = 3) shows a talovite-like phase and higher conversion after reduction at 400–450 °C, under all reaction temperatures and space velocities tested.

The catalyst with the highest amount of Al (Ni^{2+}/Al^{3+} = 0.5), and, of course, the lowest amount of nickel, shows high methanation activity, at 260 °C only after reduction at a high temperature (higher than 500 °C), in order to reduce the $NiAl_2O_4$ species.

The hydrotalcite material seems to be a promising support for Ni catalysts due to the possibility of hosting a large amount of catalyst (metal) without losing the important peculiarity of high particle size dispersion. The great quantity of aluminum present in these materials must be taken into account because it affects the reducibility of species that are formed with nickel, retarding the nickel metal sintering.

Finally, Wierzbicki et al. modified the redox properties of a hydrotalcite-based catalyst by lanthanum incorporation [193]. The presence of La increases the basicity of the support and, simultaneously weakens the interactions between Ni and the Al–Mg/Hydrotalcite matrix, producing more reducible nickel species.

2.2.5. Other Supported-Nickel Catalysts

Carbon nanotubes were also investigated as nickel supports for CO_2 methanation [194]. However, they do not show innovative properties as supports for Ni catalyst because the catalytic performance of Ni–CNT is high only in the initial stage of reaction but decreases over time. As occurs for other supports, on introducing ceria on the CNTs surface the catalyst activity and stability increase, due to the promoting effect of ceria on nickel species dispersion and their reduction [195].

Recently, a synergic effect between Ni and a W–Mg mixed oxide has been reported by Yan et al. [195]. The researchers studied a series of W-doped Ni–Mg mixed oxide catalysts in CO_2 methanation, demonstrating their excellent activity, CH_4 selectivity, and stability up to 450 °C. Particularly, the maximum CO_2 conversion is attained when the W:Ni molar ratio in the final catalyst is 1:1.

W, in fact, plays an important role in the catalyst performance: its presence promotes the formation of CO_2 adsorption sites, enhancing the catalyst activity and simultaneously favoring the Ni–Mg interactions, producing very sintering-resistant Ni species, and leading to a very stable $NiWMgO_x$ catalyst.

2.2.6. Nickel–Iron-Based Catalysts

The last part of this review is entirely dedicated to catalysts active in the CO_2 methanation reaction based on Ni–Fe systems, either as alloys or ferrites. The first papers on the application of these classes of catalysts in the reaction date back to the early 1990s, and recently they have found renewed interest due to the possible ways of exploiting CO_2 for obtaining methane as a promising energy source for methane production and/or in Fischer–Tropsch Synthesis (FTS).

Recently, Merkache et al. published a scientific work in which the activity of iron catalyst in the CO_2 hydrogenation was reported [196]. They tested a mesoporous-supported iron catalyst, Fe–KIT-6, synthesized for the first time with high iron loading. The high density of the iron sites strongly improves the CO_2 methanation selectivity of the catalyst at high temperatures [196]. However, it is well known that the activity and selectivity of iron catalysts are a function not only of the iron loading but also of the oxidation state of iron atoms.

Magnetite and M(II)-bearing ferrites form a family of oxygen-deficient spinel ferrites represented by the general formula $M_xFe_{3-x}O_{4-\delta}$, where δ represents the reduction degree of the ferrite. The oxygen deficient ferrite (ODF) is formed by hydrogen reduction at 300 °C [197]:

$$M_xFe_{3-x}O_4 + \delta H_2 = M_xFe_{3-x}O_{4-\delta} + \delta H_2O.$$

ODF decomposes CO_2 to carbon and oxygen. Carbon deposits on the ferrite surface, while oxygen penetrates the lattice of the ODF; therefore, carbon reacts with H_2 to form CH_4 at 200–300 °C [198–202]. Several ferrites ($M_xFe_{3-x}O_4$ where M = Fe, Ni, Co, Cu, Zn, Mg, Mn) have been investigated The most active results are for the $Ni_xFe_{3-x}O_4$, with over 86% CH_4 yield at 200–300 °C [199,202,203].

In [197] ultrafine Ni(II) ferrite (UNF) with 36% Ni^{2+} substitution is synthesized and tested at 300 °C in CO_2 methanation. The yield of CH_4 obtained on the UNF catalyst was 1.5–6.0 times (depending of GHSV) larger than that of the nickel ferrite (NF) catalyst. Furthermore, investigations on UNFs have mainly regarded methanation by using waste heat in stationary sources such as power plants and carbon recycling systems in flue gas in LNG power plants [204,205].

From 2004 to 2007 an interesting series of papers appeared in the literature [206–209] that, starting from fundamental concepts of heterogeneous catalysis, were applied by the authors to the methanation reaction. According to [210], one of the fundamental results is the well-known volcano curve. This is obtained when the activity of catalysts, for a given reaction, is plotted as a function of a parameter related to the ability of the surface to form chemical bonds with reactants, intermediates, or products [211,212].

Starting from the point of view that several elementary reactions at metal surfaces show a linear Bronsted–Evans–Polanyi (BEP) relation [213] between the activation energy and the reaction energy,

and reactions belonging to the same class follow the same relation, Bligaard et al. [206] investigated the implications of this finding on the kinetics of surface catalyzed chemical processes.

For the scope of the present review, the analysis presented in [206] can be used to understand the volcano curve for the methanation reaction, although related only to the CO methanation (Figure 6). Secondly, such analysis deals only with the catalytic activity; for reactions where selectivity plays a role, it cannot be used.

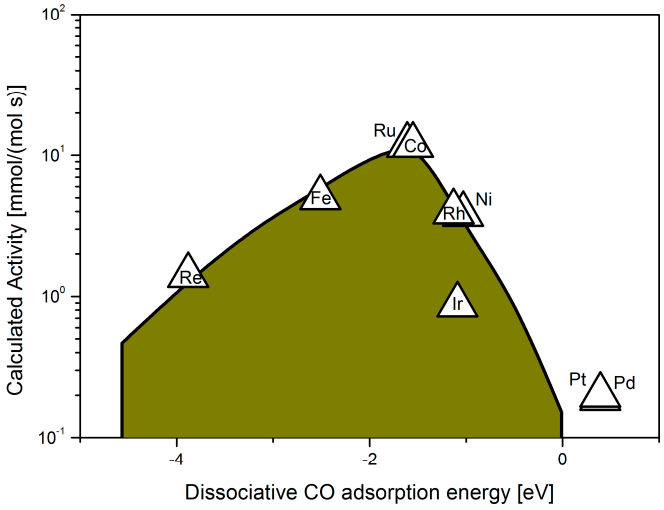

Figure 6. Activities of different supported transition metals as a function of the reaction energy for dissociative CO chemisorption at 550 K. Adapted from Bligaard et al. [206].

DFT (Density Functional Theory) is used to describe semi-quantitatively the kinetics of catalytic reactions on the basis of thermochemistry and activation energies [214–216].

Following the previous study [206], in [207] a screening of several intermetallic alloys to be used for CO methanation has been reported including experimental results. According to the authors, the two important characteristics of a catalyst surface in determining the rate of the reaction are the barrier for CO dissociation and the stability of the atomic C and O intermediates. The BEP relation reported in [207] shows the volcano dependence on the rate of E_{diss} [206]. For weak adsorption at the right in the volcano curve the barrier for dissociation is high, thus limiting the reaction rate; on the other branch (left) a strong adsorption leads to a low rate of removal of adsorbed C and O to from the reaction products. The interpolation model used in the study suggests a potential candidate for improving the methanation reaction use of alloy catalysts formed by combining the elements on the left and right branches of the curve. Moreover, a multi-objective optimization target is included in the investigation; in the economics literature, a typical solution is represented by the Pareto-optimal set [217,218].

In [207] it is clearly shown that, taking into consideration all the above reported considerations, Ni–Fe alloys have to be considered the best candidates for an "all-inclusive" material of choice for the reaction. The experimental results fully confirm the predictions from the computational screening. On the other hand, Ni–Fe alloys, also tested for CO_2 methanation, have not shown results concordant with those here discussed [219,220]. This, in our opinion, could be due to the different operational conditions adopted in the investigations.

The same approach (computational screening/experimental verifications) was followed in [208] for both CO_2 hydrogenation and simultaneous CO and CO_2 hydrogenation. The former reaction was carried out at 250 °C with a gas mixture containing 9% CO_2 in 91% H_2. The latter was conducted with a gas containing 2% CO, 2% CO_2, and 96% H_2 at 220–230 °C. It has been shown that the conversion of CO_2 to methane is significantly higher over the Ni–Fe alloy catalyst in comparison to pure Ni. For the simultaneous CO–CO_2 hydrogenation, the best catalysts have a Ni/Fe ratio >1. However, the pure Fe catalyst shows a lower activity than pure Ni.

In the last study of the series [209], some mono- and bi-metallic Ni–Fe catalysts supported on $MgAl_2O_4$ and Al_2O_3 were tested in CO methanation (reaction conditions: 2% vol. CO in H_2, 25,000 h^{-1} GHSV, reduction at 500 °C in CO/H_2 mixture for 4 h, reaction temperature in the range 200–300 °C).

Bimetallic catalysts with compositions 25Fe75Ni and 50Fe50Ni show better activity compared with monometallic Ni and Fe catalysts. The selectivity to CH_4 was found to increase at higher CO conversions and higher Ni loading in the catalysts. The maximum catalytic activity and the highest selectivity to methane are observed for a 20 wt % total metal loading on $MgAl_2O_4$.

DFT was recently applied to investigate the three different mechanisms of CO_2 methanation on Ni(111) surfaces with and without formation of CO as an intermediate [221]. The three mechanisms fall into two categories [222–224]: conversion of CO_2 to CO prior to methanation involving a CO intermediate [225,226], and direct hydrogenation of CO_2 to methane without the formation of CO as an intermediate [63,127,227,228].

On the basis of the calculated energy barrier values for each of the three paths and the correlated determination of the rate determining step (r.d.s.), path 2 (the decomposition of CO_2 into CO and O, further decomposition of CO into C and O (r.d.s), and hydrogenation of C to CH_4)) appears to be the most accredited mechanism.

Other recent relevant studies devoted to Ni–Fe-based catalysts for methanation reactions regarded the effect of the Fe content on Al_2O_3-supported catalysts in the co-methanation of CO and CO_2 [229]; the influence of the second metal for CO hydrogenation [230]; the effect of the preparation method [231]; and the effect of the addition of a noble metal (Ru) [232] on the activity and selectivity of the reactions investigated.

In [229] the maximum carbon conversion and CH_4 selectivity on Ni_xFe_{1-x}/Al_2O_3 (20 wt % metal content on the support) was observed for the $Ni_{0.7}Fe_{0.3}/Al_2O_3$ catalyst. Higher Fe content causes a decrease in C conversion and CH_4 productivity because of the occurrence of WGS reaction and C_2–C_5 hydrocarbon formation.

Alumina xerogel (AX)—used as a support of Ni catalysts with the addition of a second metal M (M = Fe, Ni, Co, Ce, La)—was tested in CO hydrogenation (feed composition $CO:H_2:N_2$ = 1:3:1.7) at 230 °C and 10 bar. Both CO conversion and CH_4 yield decrease in the order 30Ni10FeAX > 30Ni10NiAX > 30Ni10CoAX > 30Ni10CeAX > 30Ni10LaAX. The low performance exhibited by both Ce and La as a second metal appears to denote that transition metals (Fe, Co, Ni) are more effective in promoting the reaction than lanthanides (Ce, La). Moreover, on the basis of temperature-programmed surface reaction (TPSR) experiments, the higher performance of 30Ni10FeAX was attributed to the optimal CO dissociation energy and the largest H_2 adsorption [230]. Following the latter two studies discussed above, Hwang et al. investigated, on the same catalytic system (AX-supported Ni-Fe), the effect of the precipitation agent, on the catalysts prepared by coprecipitation, on methane production from CO_2 and H_2. The precipitation agent used ($(NH_4)_2CO_3$, Na_2CO_3, NH_4OH, or NaOH) has a decisive role on the catalytic performance since it influences the extent of the active surface area. Therefore, among the catalysts tested, NiFeAl-$(NH_4)_2CO_3$, affording the smallest particle size, shows the best results in terms of CO_2 conversion and CH_4 yield [231].

The alumina xerogel support was again used to investigate the effect of the addition of different ruthenium contents (x = 0, 0.2, 0.4, 0.6, 0.8, 1.0) on the activity of the same reaction; in operative conditions the feed composition is $CO_2:H_2:N_2$ = 1:4:1.7, P = 10 bar, T = 220 °C. A close correlation between the metal surface area and the amount of desorbed CO_2 (measured by CO_2–TPD) was found. Both CO_2 conversion and CH_4 yield show a well-defined volcano-shaped trend with respect to Ru content. Furthermore, the CH_4 yield increases on increasing the metal surface area and the amount of desorbed CO_2 [232].

Bimetallic Ni–Fe catalysts were tested in the CO methanation reaction for the production of substitute natural gas (SNG) under industrial (0.1–0.3 MPa) total methanation conditions to be adopted in processes related to the Fischer–Tropsch synthesis [232–236]. Thus, in [5] the activity of bimetallic Ni_3Fe/γ-Al_2O_3 was first compared with that of a reference Ni/γ-Al_2O_3 under conditions

of 3.0 MPa and H_2/CO = 3.1. Ni_3Fe/γ-Al_2O_3 achieves the 100% CO conversion at 225 °C, whereas Ni/γ-Al_2O_3 reaches total CO conversion at 275 °C. Also, in the high temperature range of 500–600 °C, the CO conversion of the bimetallic catalyst is higher than that of the monometallic catalyst, with 99% selectivity to CH_4 from 300 °C to 450 °C. The influence of the Ni/Fe ratio on the catalytic activity of a number of bimetallic Ni–Fe catalysts in CO methanation at 0.1 MPa was also investigated. $Ni_3Fe_{1.8}/\gamma$-Al_2O_3 shows the lowest CO conversion and CH_4 selectivity, even lower than that of Ni/γ-Al_2O_3. Clearly, the higher Fe content is responsible for the poor catalyst performance. Comparing all the results obtained in high-pressure methanation test with the low-pressure experiments reported in [5], Tian et al. conclude that the performance of Ni–Fe catalysts is not determined by the content of individual Ni or Fe, but by the synergistic effect of the two metals in the catalyst. Another process able to produce CH_4 has been reported to be the decomposition of CO_2 to carbon and oxygen [237–240]. In this regard, ferrite catalysts have been previously used for this reaction and being non-stoichiometric or oxygen-deficient materials are able to decompose water to hydrogen and CO_2 to carbon [241–245].

In [246] the decomposition of CO_2 was carried out on the nanophase $NiFe_2O_4$ (NFN, $Ni_xFe_{3-x}O_{4-\delta}$, $0 < \delta < 1$) at 300 °C to obtain CO, CO_2, or CH_4. After the CO_2 decomposition, the reactor was flushed with hydrogen to carry out the methanation process. The two reaction routes for decomposing CO_2 by oxygen-deficient ferrites are: (i) decomposition to carbon and oxygen; (ii) decomposition into carbon monoxide and oxygen [247–251].

The experimental results reported in [246] clearly show that the prepared NFNs were effective at decomposing CO_2 into carbon and oxygen after reduction by hydrogen. In conclusion, the overall mechanism of CO_2 decomposition over $NiFe_2O_4$ nanoparticles can be summarized as follows: (i) H_2 gas decomposes and produces the water molecule, making the $NiFe_2O_4$ oxygen-deficient; (ii) the oxygen-deficient $NiFe_2O_4$ adsorbs oxygen atoms from CO_2 and produces carbon on the surface or CO when $NiFe_2O_4$ is less active; (iii) the produced carbon reacts with H_2 and produces CH_4 by methanation.

A new interesting iron source for supported bimetallic Ni–Fe catalysts preparation has recently been proposed by Wang et al. [252], and consists of using calcined olivine as a promising Ni support for CO_2 methanation. Before this study, the activity of calcined olivine supported nickel has been demonstrated in gasification [253] and steam reforming [254] of biomass. Olivine is a magnesium iron silicate with the general formula $(Mg_xFe_{1-x})_2SiO_4$ and is a common Earth mineral. The peculiarity of the support consists in the possibility of allowing interaction between NiO and olivine structure to lead to a better dispersion of Ni species. This effect is promoted by the simultaneous presence of iron and MgO. First of all, Wang et al. describe the effect of the support calcination on iron species. They observed that iron was extracted by the olivine structure during the calcination process so that more reducible iron species can be formed (analyzed by usual TPR experiments). The amount of reducible iron species increases on increasing the temperature to 800 °C. Form 800 °C to 1200 °C a reversal trend was registered, probably due to the reintegration of extracted iron into the olivine structure. Over 1200 °C the reducible iron amount increases again and $MgSiO_3$ species are formed, as confirmed by the XRD spectrum. TPR profiles of Ni/olivine catalysts obtained by calcining the support at different temperatures show that for the catalyst calcined at lower temperature nickel is just deposited on the olivine structure with a weak interaction as highly dispersed particles. On the contrary, for catalysts calcined at temperatures >900 °C, a NiO–MgO solid solution phase and grafted NiO species were formed. The best catalyst, obtained by calcination of the support at 350 °C and reduction at 500 °C, is able to reach, under tested conditions, a CO_2 conversion of 98.4% and a CH_4 selectivity of 99.9%.

Important and very recent results that confirm the role of iron on the dispersion of NiO nanoparticles, increasing the quantity of the reduced active nickel species, were reported by Lu et al. regarding zirconia-supported doped nickel catalysts [255] and Pandey et al., regarding five series of Ni–Fe bimetallic supported catalysts [256]. The morphology of $Ni–ZrO_2$ and $Ni–Fe/ZrO_2$ catalysts

has been compared. Using TEM images, it is possible to notice that the average size of NiO particles on the Ni–ZrO_2 catalyst is higher than the average size of the NiO particles dispersed on Ni–Fe/ZrO_2 catalyst [255].

3. Industrial Applications and Concluding Remarks

The use of carbon dioxide as a feedstock for fuels, and for energy in general, is a promising route that permits adherence to main international protocols on environmental protection. Hydrogenation is an appropriate way to reduce CO_2 and provide a range of substances compatible with existent technologies. The methane produced in this way could be directly injected into already existent pipeline networks or storage infrastructures. Obviously, the main challenge that ensures an environmentally friendly process is obtaining hydrogen from renewable sources and energy. Water electrolysis promoted by renewable energy (wind, solar, etc.) is an economic and clean method of H_2 production. Hydrogen can be directly injected into a natural gas grid or combined with CO_2 by a methanation process.

Energy production by these ways is the basis of the *Power-to-Gas* concept (P2G). However, currently, this is only a model: there are demo-plants and industrial-scale plants that demonstrate the possibility of producing energy by gas. Germany seems to be at the cutting edge in the P2G technology that provides SNG (Substitute or Synthetic Natural Gas) as a product, since 2009.

In Stuttgard there is a demonstration *Power-to-methane* plant (250 kW power input as capacity) founded by ZSW (the Center for Solar Energy and Hydrogen Research) by ETOGAS GmbH. ETOGAS, in Wertle, Germany, is an industrial-scale *Power-to-methane* plant (6300 kW power input as capacity) that produces methane for Audi. The produced methane, named *Audi-e-gas*, comes from the CO_2 obtained by a waste-biogas plant.

More recently, the Karlsruhe Institute of Technology (KIT) coordinated the innovative HELMETH project (Integrated High-Temperature Electrolysis and Methanation for Effective Power to Gas Conversion) [257]. The project, co-financed by the EU's Seventh Framework Program, has the objective of proving the highly efficient Power-to-Gas (P2G) technology by thermally integrating high-temperature electrolysis (SOEC Technology) with methanation. The expected efficiency should be higher than 85%, superior to the efficiency for hydrogen generation via conventional water electrolysis. In practice, high-temperature electrolysis (endothermic) and methanation (exothermic) can be coupled and thermally integrated with increasing globally conversion efficiency.

At the same time, the Electrochaea Company has developed a commercial power-to gas system solution using a microorganism (methanogenic archaea) as biocatalyst, patented as BioCat, for a methanation technology to operate at lower costs and with higher flexibility than conventional thermochemical methanation processes [258]. Archaea BioCat exhibits several properties including high mass conversion efficiency and high tolerance to many contaminants typically present in industrial CO_2 sources, such as O_2, H_2S and particulates that can poison common catalysts. Moreover, archaea are highly selective towards methane formation, so minimal post-reaction gas treatment is needed before injecting the produced gas into the gas grid. The power-to-gas technology of the Electrochaea system uses an electrolyzer to produce hydrogen, which is fed into a bioreactor containing the archaea along with carbon dioxide from a biogenic (anaerobic digesters, fermentation plants) or industrial source (fuel gas from combustion processes). In February 2014, Electrochaea began its first commercial-scale demonstration project BioCat: a 1 MW power-to-gas plant based on biological methanation.

High flexibility, reduced technological cost, and high process efficiency make biomethanation technology an attractive source of renewable energy. The global evaluation of biomethanation assets should also include the Life Cycle Sustainability Assessment (LSCA) methodology. Kristjanpoller et al. have published an interesting work on the biomethanation plant assessment [259]. The work pinpoints two important concepts that will guide research and generate proposals for industrial plant improvement: effectiveness and efficiency. The first is related to the extent to which the objectives of the process are met; the second is the measure of the economy in which the resources of the company are used, including the cost of the catalyst.

In any case, even if the mechanism that currently promotes methanation on nanosized metal catalysts, as well as the best-performing catalyst system and the effectiveness of industrial power-to-gas plants are under scientific debate, we can say without a doubt that the commercialization of CO_2 methanation processes plays a pivotal role in the future of environmentally friendly energy systems.

Author Contributions: All authors contributed to write the paper.

Conflicts of Interest: The authors declare no conflict of interest.

References

1. Iglesias, G.M.; de Vries, C.; Claeys, M.; Schaub, G. Chemical energy storage in gaseous hydrocarbons via iron Fischer–Tropsch synthesis from H_2/CO_2-Kinetics, selectivity and process considerations. *Catal. Today* **2015**, *242*, 184–192. [CrossRef]
2. Janke, C.; Duyar, M.S.; Hoskins, M.; Farrauto, R. Catalytic and adsorption studies for the hydrogenation of CO_2 to methane. *Appl. Catal. B Environ.* **2014**, *152–153*, 184–191. [CrossRef]
3. Koschany, F.; Schelereth, D.; Hinrichsen, O. On the kinetics of the methanation of carbon dioxide on coprecipitated $NiAl(O)_x$. *Appl. Catal. B Environ.* **2016**, *181*, 504–516. [CrossRef]
4. Ashok, J.; Ang, M.L.; Kawi, S. Enhanced activity of CO_2 methanation over Ni/CeO_2–ZrO_2 catalysts: Influence of preparation method. *Catal. Today* **2017**, *281*, 304–311. [CrossRef]
5. Tian, D.; Liu, Z.; Li, D.; Shi, H.; Pan, W.; Cheng, Y. Bimetallic Ni-Fe total-methanation catalyst for the production of substitute natural gas under high pressure. *Fuel* **2013**, *104*, 224–229. [CrossRef]
6. Abelló, S.; Berrueco, C.; Montané, D. High-loaded nickel–alumina catalyst for direct CO_2 hydrogenation into synthetic natural gas (SNG). *Fuel* **2013**, *113*, 598–609. [CrossRef]
7. Tao, M.; Xin, Z.; Meng, X.; Bian, Z.; Lv, Y. Highly dispersed nickel within mesochannels of SBA-15 for CO methanation with enhanced activity and excellent thermostability. *Fuel* **2017**, *188*, 267–276. [CrossRef]
8. Schaaf, T.; Grünig, J.; Roman Schuster, M.; Rothenfluh, T.; Orth, A. Methanation of CO_2—Storage of renewable energy in a gas distribution system. *Energy Sustain. Soc.* **2014**, 2–14. [CrossRef]
9. Sahebdelfar, S.; Ravanchi, M.T. Carbon dioxide utilization for methane production: A thermodynamic analysis. *J. Pet. Sci. Eng.* **2015**, *134*, 14–22. [CrossRef]
10. Su, X.; Xu, J.; Liang, B.; Duan, H.; Hou, B.; Huang, Y. Catalytic carbon dioxide hydrogenation to methane: A review of recent studies. *J. Energy Chem.* **2016**, *25*, 553–565. [CrossRef]
11. Ronsch, S.; Schneider, J.; Matthischke, S.; Schluter, M.; Gotz, M.; Lefebre, J.; Prabhakaran, P.; Bajohr, S. Review on methanation—From fundamentals to current projects. *Fuel* **2016**, *166*, 276–296. [CrossRef]
12. Aziz, M.A.A.; Jalil, A.A.; Triwahyono, S.; Ahmad, A. CO_2 methanation over heterogeneous catalysts: Recent progress and future prospects. *Green Chem.* **2015**, *17*, 2647–2663. [CrossRef]
13. Puga, A.V. Light-Promoted Hydrogenation of Carbon dioxide—An overview. *Top. Catal.* **2016**, *59*, 1268–1278. [CrossRef]
14. Wang, W.; Gong, J. Methanation of carbon dioxide: An overview. *Front. Chem. Sci. Eng.* **2011**, *5*, 2–10.
15. Liu, J.X.; Hou, W.H. Study on Ru-based catalyst used in reductive reaction of CO_2. *Space Med. Med. Eng.* **2004**, *17*, 457–460.
16. Meng, Y.Y.; Shang, C.X. A study on CO_2 methanization reduction technology. *Space Med. Med. Eng.* **1994**, *7*, 115–120.
17. Zhou, K.H.; Wu, B.Z.; Ren, C.B. Comparative analysis of Sabatier CO_2 reduction system for space station. *Space Med. Med. Eng.* **2011**, *24*, 384–390.
18. Liu, C.; Cundari, T.R.; Wilson, A.K. CO_2 reduction on transition metal (Fe, Co, Ni, and Cu) surface: In comparison with homogeneous catalysis. *J. Phys. Chem. C.* **2012**, *116*, 5681–5688. [CrossRef]
19. Choe, S.J.; Park, D.H.; Huh, D.S. Adsorption and dissociation reaction of carbon dioxide on Pt(111) and Fe(111) surface: MO-study. *Bull. Korean Chem. Soc.* **2000**, *21*, 779–784.
20. Solymosi, F. The bonding, structure and reaction of CO_2 adsorbed on clean and promoted metal surface. *J. Mol. Catal.* **1991**, *65*, 337–358. [CrossRef]
21. Fechete, I.; Vedrine, J.V. Nanoporous materials as new engineered catalysts for the synthesis of green fuels. *Molecules* **2015**, *20*, 5638–5666. [CrossRef] [PubMed]

22. Italiano, G.; Espro, C.; Arena, F.; Frusteri, F.; Parmaliana, A. Catalytic features of Mg modified Ni/SiO_2/Silica cloth systems in the decomposition of methane for making CO_x-Free Hydrogen. *Catal. Lett.* **2008**, *124*, 7–12. [CrossRef]
23. Frontera, P.; Aloise, A.; Macario, A.; Crea, F.; Antonucci, P.L.; Giordano, G.; Nagy, J.B. Zeolite-supported Ni catalyst for methane reforming with carbon dioxide. *Res. Chem. Intermed.* **2011**, *37*, 267–279. [CrossRef]
24. Mauriello, F.; Vinci, A.; Espro, C.; Gumina, B.; Musolino, M.G.; Pietropalo, R. Hydrogenolysis vs. aqueous phase reforming (APR) of glycerol promoted by a heterogeneous Pd/Fe catalyst. *Catal. Sci. Technol.* **2015**, *5*, 4466–4473. [CrossRef]
25. Frontera, P.; Macario, A.; Aloise, A.; Antonucci, P.L.; Giordano, G.; Nagy, J.B. Effect of support surface on methane dry-reforming catalyst preparation. *Catal. Today* **2013**, *218–219*, 18–29. [CrossRef]
26. Candamano, S.; Frontera, P.; Macario, A.; Crea, F.; Nagy, J.B. Preparation and characterization of active Ni-supported catalyst for syngas production. *Chem. Eng. Res. Des.* **2015**, *96*, 78–86. [CrossRef]
27. Breen, J.P.; Burch, R.; Coleman, H.M. Metal-catalyzed steam reforming of ethanol in the production of hydrogen for fuel cell application. *Appl. Catal. B Environ.* **2002**, *39*, 65–74. [CrossRef]
28. Pompeo, F.; Nichio, N.N.; Feretti, O.A.; Resasco, D. Study of Ni catalysts on different supports to obtain synthesis gas. *Int. J. Hydrogen Energy* **2005**, *30*, 1399–1405. [CrossRef]
29. Lo Faro, M.; Frontera, P.; Antonucci, P.L.; Aricò, A.S. Ni-Cu based catalysts prepared by two different methods and their catalytic activity toward the ATR of methane. *Chem. Eng. Res. Des.* **2015**, *93*, 269–277. [CrossRef]
30. Jacquemin, M.; Beuls, A.; Ruiz, P. Catalytic production of methane from CO_2 and H_2 at low temperature: Insight on the reaction mechanism. *Catal. Today* **2010**, *157*, 462–466. [CrossRef]
31. Beuls, A.; Swalus, C.; Jacquemin, M.; Heyen, G.; Karelovic, A.; Ruiz, P. Methanation of CO_2: Further insight into the mechanism over Rh/γ-Al_2O_3 catalyst. *Appl. Catal. B Environ.* **2012**, *113–114*, 2–10. [CrossRef]
32. Karelovic, A.; Ruiz, P. CO_2 hydrogenation at low temperature over Rh/γ-Al_2O_3 catalysts: Effect of the metal particle size on catalytic performances and reaction mechanism. *Appl. Catal. B Environ.* **2012**, *113–114*, 237–249. [CrossRef]
33. Wijayapalaa, R.; Yu, F.; Pittman, C.U., Jr.; Mlsna, T.T. K-promoted Mo/Co- and Mo/Ni-catalyzed Fischer–Tropsch synthesis of aromatic hydrocarbons with and without a Cu water gas shift catalyst. *Appl. Catal. A Gen.* **2014**, *480*, 93–99. [CrossRef]
34. Swalus, C.; Jacquemin, M.; Poleunis, C.; Bertrand, P.; Ruiz, P. CO_2 methanation on Rh/γ-Al_2O_3 catalyst at low temperature: "In situ" supply of hydrogen by Ni/activated carbon catalyst. *Appl. Catal. B Environ.* **2012**, *125*, 41–50. [CrossRef]
35. Karelovic, A.; Ruiz, P. Mechanistic study of low temperature CO_2 methanation over Rh/TiO_2 catalysts. *J. Catal.* **2013**, *301*, 141–153. [CrossRef]
36. Solymosi, F.; Erdöhelyi, A.; Bánsági, T. Methanation of CO_2 on supported rhodium catalyst. *J. Catal.* **1981**, *68*, 371–382. [CrossRef]
37. Zhang, Z.L.; Kladi, A.; Verykios, X.E. Effects of Carrier Doping on Kinetic Parameters of CO_2 Hydrogenation on Supported Rhodium Catalysts. *J. Catal.* **1994**, *148*, 737–747. [CrossRef]
38. Solymosi, F.; Tombácz, I.; Koszta, J. Effects of variation of electric properties of TiO_2 support on hydrogenation of CO and CO_2 over Rh catalysts. *J. Catal.* **1985**, *95*, 578–586. [CrossRef]
39. Bell, A.T. The influence of metal oxides on the activity and selectivity of transition metal catalysts. *J. Mol. Catal. A* **1995**, *100*, 1–11.
40. Williams, K.J.; Boffa, A.B.; Salmeron, M.; Bell, A.T.; Somorjai, G.A. The kinetics of CO_2 hydrogenation on a Rh foil promoted by Titania overlayers. *Catal. Lett.* **1991**, *9*, 415426. [CrossRef]
41. Trovarelli, A.; Deleitenburg, C.; Dolcetti, G.; Lorca, J.L. CO_2 Methanation under Transient and Steady-State Conditions over Rh/CeO_2 and CeO_2-Promoted Rh/SiO_2: The Role of Surface and Bulk Ceria. *J. Catal.* **1995**, *151*, 111–124. [CrossRef]
42. Deleitenburg, C.; Trovarelli, A. Metal-Support Interactions in Rh/CeO_2, Rh/TiO_2, and Rh/Nb_2O_5 Catalysts as Inferred from CO_2 Methanation Activity. *J. Catal.* **1995**, *156*, 171–174. [CrossRef]
43. Ma, S.; Song, W.; Liu, B.; Zheng, H.; Deng, J.; Zhong, W.; Liu, J.; Gong, X.Q.; Zhao, Z. Elucidation of the high CO_2 reduction selectivity of isolated Rh supported on TiO_2: A DFT study. *Catal. Sci. Technol.* **2016**, *6*, 6128–6136. [CrossRef]

44. Fukui, K.; Yonezawa, T.; Shingu, H. A molecular Orbital Theory of Reactivity in Aromatic Hydrocarbons. *J. Chem. Phys.* **1952**, *20*, 722–725. [CrossRef]
45. Kusmierz, M. Kinetic study on carbon dioxide hydrogenation over Ru/γ-Al_2O_3 catalysts. *Catal. Today* **2008**, *137*, 429–432. [CrossRef]
46. Mills, G.A.; Steffgen, F.W. Catalytic Methanation. *Catal. Rev.* **1974**, *8*, 159–210. [CrossRef]
47. Weatherbee, G.D.; Bartholomew, C.H. Hydrogenation of CO_2 on group VIII metals: IV. Specific activities and selectivities of silica-supported Co, Fe, and Ru. *J. Catal.* **1984**, *87*, 352–362. [CrossRef]
48. Sugawa, S.; Sayama, K.; Okabe, K.; Arakawa, H. Methanol synthesis from CO_2 and H_2 over silver catalyst. *Energy Convers. Manag.* **1995**, *36*, 665–668. [CrossRef]
49. Scirè, S.; Crisafulli, C.; Maggiore, R.; Minicò, S.; Galvagno, S. Influence of the support on CO_2 methanation over Ru catalysts: An FT-IR study. *Catal. Lett.* **1998**, *51*, 41–45. [CrossRef]
50. Li, D.; Ichikuni, N.; Shimazu, S.; Uematsu, T. Catalytic properties of sprayed Ru/Al_2O_3 and promoter effects of alkali metals in CO_2 hydrogenation. *Appl. Catal. A Gen.* **1998**, *172*, 351–358. [CrossRef]
51. Li, D.; Ichikuni, N.; Shimazu, S.; Uematsu, T. Hydrogenation of CO_2 over sprayed Ru/TiO_2 fine particles and strong metal-support interaction. *Appl. Catal. A Gen.* **1999**, *180*, 227–235. [CrossRef]
52. Toemen, S.; Bakar, W.A.W.A.; Ali, R. Effect of ceria and strontian over Ru/Mn/Al_2O_3 catalyst: Catalytic methanation, physicochemical and mechanistic studies. *J. CO_2 Util.* **2016**, *13*, 38–49. [CrossRef]
53. Garbarino, G.; Bellotti, D.; Riani, P.; Magistri, L.; Busca, G. Methanation of carbon dioxide on Ru/Al_2O_3 and Ni/Al_2O_3 catalysts at atmospheric pressure: Catalysts activation, behaviour and stability. *Int. J. Hydrogen Energy* **2015**, *40*, 9171–9182. [CrossRef]
54. Garbarino, G.; Bellotti, D.; Finocchio, E.; Magistri, L.; Busca, G. Methanation of carbon dioxide on Ru/Al_2O_3: Catalytic activity and infrared study. *Catal. Today* **2016**, *277*, 21–28. [CrossRef]
55. Kowalczyk, Z.; Stołecki, K.; Raròg-Pilecka, W.; Miskiewicz, E.; Wilczkowska, E.; Karpinski, Z. Supported ruthenium catalysts for selective methanation of carbon oxides at very low CO_x/H_2 ratios. *Appl. Catal. A Gen.* **2008**, *342*, 35–39. [CrossRef]
56. Li, T.; Wang, S.; Gao, D.; Wang, S. Effect of support calcination temperature on the catalytic properties of Ru/$Ce_{0.8}Zr_{0.2}O_2$ for methanation of carbon dioxide. *J. Fuel Chem. Technol.* **2014**, *42*, 1440–1446. [CrossRef]
57. Akamarua, S.; Shimazaki, T.; Kuboc, M.; Abe, T. Density functional theory analysis of methanation reaction of CO_2 on Ru nanoparticle supported on TiO_2 (101). *Appl. Catal. A Gen.* **2014**, *470*, 405–411. [CrossRef]
58. Ravindranathan Thampi, K.; Kiwi, J.; Grätzel, M. Methanation and photo-methanation of carbon dioxide at room temperature and atmospheric pressure. *Nature* **1987**, *327*, 506–508. [CrossRef]
59. Gupta, N.M.; Kamble, V.S.; Kartha, V.B.; Iyer, R.M.; Ravindranathan Thampi, K.; Gratzel, M. FTIR spectroscopic study of the interaction of CO_2 and CO_2 + H_2 over partially oxidized $RuTiO_2$ catalyst. *J. Catal.* **1994**, *146*, 173–184. [CrossRef]
60. Abe, T.; Tanizawa, M.; Watanabe, K.; Taguchi, A. CO_2 methanation property of Ru nanoparticle-loaded TiO_2 prepared by a polygonal barrel-sputtering method. *Energy Environ. Sci.* **2009**, *2*, 315–321. [CrossRef]
61. Xu, J.; Su, X.; Duan, H.; Hou, B.; Lin, Q.; Liu, X.; Pan, X.; Pei, G.; Geng, H.; Huang, Y.; et al. Influence of pretreatment temperature on catalytic performance of rutile TiO_2-supported ruthenium catalysts in CO_2 methanation. *J. Catal.* **2016**, *333*, 227–237. [CrossRef]
62. Tada, S.; Ochienga, O.J.; Kikuchi, R.; Haneda, T.; Kameyama, H. Promotion of CO_2 methanation activity and CH_4 selectivity at low temperatures over Ru/CeO_2/Al_2O_3 catalysts. *Int. J. Hydrogen Energy* **2014**, *39*, 10090–10100. [CrossRef]
63. Sharma, S.; Hu, Z.; Zhang, P.; McFarland, E.W.; Metiu, H. CO_2 methanation on Ru-doped ceria. *J. Catal.* **2011**, *278*, 297–309. [CrossRef]
64. Xu, J.; Lin, Q.; Su, X.; Duan, H.; Geng, H.; Huang, Y. CO_2 Methanation over TiO_2-Al_2O_3 Binary Oxides Supported Ru Catalysts. *Chin. J. Chem. Eng.* **2016**, *24*, 140–145. [CrossRef]
65. Zamani, A.H.; Ali, R.; Bakar, W.A.W.A. Optimization of CO_2 methanation reaction over M*/Mn/Cu–Al_2O_3 (M*: Pd, Rh and Ru) catalysts. *J. Ind. Eng. Chem.* **2015**, *29*, 238–248. [CrossRef]
66. Zamani, A.H.; Ali, R.; Bakar, W.A.W.A. The investigation of Ru/Mn/Cu–Al_2O_3 oxide catalysts for CO_2/H_2 methanation in natural gas. *J. Tawain Inst. Chem. Eng.* **2014**, *45*, 143–152. [CrossRef]
67. Toemen, S.; Bakar, W.A.W.A.; Ali, R. Investigation of Ru/Mn/Ce/Al_2O_3 catalyst for carbon dioxide methanation: Catalytic optimization, physicochemical studies and RSM. *J. Tawain Inst. Chem. Eng.* **2014**, *45*, 2370–2378. [CrossRef]

68. Borodziński, A.; Bond, G.C. Selective Hydrogenation of Ethyne in Ethene-Rich Streams on Palladium Catalysts. Part 1. Effect of Changes to the Catalyst During Reaction. *Catal. Rev. Sci. Eng.* **2006**, *48*, 91–144. [CrossRef]
69. Albers, P.; Pietsch, J.; Parker, S.F. Poisoning and deactivation of palladium catalysts. *J. Mol. Catal. A Chem.* **2001**, *173*, 275–286. [CrossRef]
70. Schuurman, Y.; Mirodatos, C.; Ferreira-Aparicio, P.; Rodriguez-Ramos, I.; Guerrero-Ruiz, A. Bifunctional pathways in the carbon dioxide reforming of methane over MgO-promoted Ru/C catalysts. *Catal. Lett.* **2000**, *66*, 33–37. [CrossRef]
71. Galuszka, J. Carbon dioxide chemistry during oxidative coupling of methane on a Li/MgO catalyst. *Catal. Today* **1994**, *21*, 321–331. [CrossRef]
72. Chen, Y.; Tomishige, K.; Yokoyama, K.; Fujimoto, K. Promoting effect of Pt, Pd and Rh noble metals to the $Ni_{0.03}Mg_{0.97}O$ solid solution catalysts for the reforming of CH_4 with CO_2. *Appl. Catal. A Gen.* **1997**, *165*, 335–347. [CrossRef]
73. Veith, G.M.; Lupini, A.R.; Rashkeev, S.; Pennycook, S.J.; Mullins, D.R.; Schwartz, V.; Bridges, C.A.; Dudney, N.J. Thermal stability and catalytic activity of gold nanoparticles supported on silica. *J. Catal.* **2009**, *262*, 92–101. [CrossRef]
74. Martins, J.; Batail, N.; Silva, S.; Rafik-Clement, S.; Karelovic, A.; Debecker, D.P.; Chaumonnot, A.; Uzio, D. CO_2 hydrogenation with shape-controlled Pd nanoparticles embedded in mesoporous silica: Elucidating stability and selectivity issues. *Catal. Commun.* **2015**, *58*, 11–15. [CrossRef]
75. Delmelle, R.; Duarte, R.B.; Franken, T.; Burnat, D.; Holzer, L.; Borgschulte, A. Development of improved nickel catalysts for sorption enhanced CO_2 methanation. *Int. J. Hydrogen Energy* **2015**, *41*, 20185–20191. [CrossRef]
76. Vaudagna, S.R.; Comelli, R.A.; Figoli, N.S. Influence of the tungsten oxide precursor on WO_x-ZrO_2 and Pt/WO_x-ZrO_2 properties. *Appl. Catal. A Gen.* **1997**, *164*, 265–280. [CrossRef]
77. Chang, F.W.; Kuo, M.S.; Tsay, M.T.; Hsieh, M.C. Hydrogenation of CO_2 over nickel catalysts on rice husk ash-alumina prepared by incipient wetness impregnation. *Appl. Catal. A Gen.* **2003**, *247*, 309–320. [CrossRef]
78. Gao, J.; Jia, C.; Li, J.; Zhang, M.; Gua, F.; Xua, G.; Zhong, Z.; Sua, F. Ni/Al_2O_3 catalysts for CO methanation: Effect of Al_2O_3 supports calcined at different temperatures. *J. Energy Chem.* **2013**, *22*, 919–927. [CrossRef]
79. Takenaka, S.; Shimizu, T.; Otsuka, K. Complete removal of carbon monoxide in hydrogen-rich gas stream through methanation over supported metal catalysts. *Int. J. Hydrogen Energy* **2004**, *29*, 1065–1073. [CrossRef]
80. Danaci, S.; Protasova, L.; Lefevere, J.; Bedel, L.; Guilet, R.; Marty, P. Efficient CO_2 methanation over Ni/Al_2O_3 coated structured catalysys. *Catal. Today* **2016**, *273*, 234–243. [CrossRef]
81. Tada, S.; Shimizu, T.; Kameyama, H.; Haneda, T.; Kikuchi, R. Ni/CeO_2 catalysts with high CO_2 methanation activity and high CH_4 selectivity at low temperatures. *Int. J. Hydrogen Energy* **2012**, *37*, 5527–5531. [CrossRef]
82. Song, H.; Yang, J.; Zhao, J.; Chou, L. Methanation of carbon dioxide over a highly dispersed Ni/La_2O_3 catalyst. *Chin. J. Catal.* **2010**, *31*, 21–23. [CrossRef]
83. Zhang, L.; Li, L.; Zhang, Y.; Zhao, Y.; Li, J. Nickel catalysts supported on MgO with different specific surface area for carbon dioxide reforming of methane. *J. Energy Chem.* **2014**, *23*, 66–72. [CrossRef]
84. Fukuhara, C.; Hayakawa, K.; Suzuki, Y.; Kawasaki, W.; Watanabe, R. A novel nickel-based structured catalyst for CO_2 methanation: A honeycomb-type Ni/CeO_2 catalyst to transform greenhouse gas into useful resource. *Appl. Catal. A Gen.* **2017**, *532*, 12–18. [CrossRef]
85. Aksoylu, A.E.; Önsan, Z.I. Hydrogenation of carbon oxides using coprecipitated and impregnated Ni/Al_2O_3 catalysts. *Appl. Catal. A Gen.* **1997**, *164*, 1–11. [CrossRef]
86. Zhou, R.; Rui, N.; Fan, Z.; Liu, C. Effect of the structure of Ni/TiO_2 catalyst on CO_2 methanation. *Int. J. Hydrogen Energy.* **2016**, *41*, 22017–22025. [CrossRef]
87. Da Silva, D.C.D.; Letichevsky, S.; Borges, L.E.P.; Appel, L.G. The Ni/ZrO_2 catalyst and the methanation of CO and CO_2. *Int. J. Hydrogen Energy* **2012**, *37*, 8923–8928. [CrossRef]
88. Muroyama, H.; Tsuda, Y.; Asakoshi, T.; Masitah, H.; Okanishi, T.; Matsui, T.; Eguchi, K. Carbon dioxide methanation over Ni catalysts supported on various metal oxides. *J. Catal.* **2016**, *343*, 178–184. [CrossRef]
89. Takano, H.; Kirihata, Y.; Izumiya, K.; Kumagai, N.; Habazaki, H.; Hashimoto, K. Higly active Ni/Y doped Zr_2O catalyst for CO_2 methanation. *App. Surf. Sci.* **2016**, *358*, 653–663. [CrossRef]
90. Wang, S.; Lu, G.Q.M. Role of CeO_2 in Ni/CeO_2-Al_2O_3 catalysts for carbon dioxide reforming of methane. *Appl. Catal. B Environ.* **1998**, *19*, 267–277. [CrossRef]

91. Aksoylu, A.E.; Akin, A.N.; Önsan, Z.I.; Trimm, D.L. Structure/activity relationships in coprecipitated nickel-alumina catalysts using CO_2 adsorption and methanation. *Appl. Catal. A Gen.* **1996**, *145*, 185–193. [CrossRef]
92. Rahmani, S.; Rezaei, M.; Meshkania, F. Preparation of highly active nickel catalysts supported on mesoporous nanocrystalline γ-Al_2O_3 for CO_2 methanation. *J. Ind. Eng. Chem.* **2014**, *20*, 1346–1352. [CrossRef]
93. Garbarino, G.; Riani, P.; Magistri, L.; Busca, G. A study of the methanation of carbon dioxide on Ni/Al_2O_3 catalysts at atmospheric pressure. *Int. J. Hydrogen Energy* **2014**, *39*, 11557–11565. [CrossRef]
94. Mutz, B.; Carvalho, H.W.P.; Mangold, S.; Kleist, W.; Grunwaldt, J.D. Methanation of CO_2: Structural response of a Ni-based catalyst under fluctuating reaction conditions unraveled by operando spectroscopy. *J. Catal.* **2015**, *327*, 48–53. [CrossRef]
95. Weckhuysen, B.M. Determining the active site in a catalytic process: Operando spectroscopy is more than a buzzword. *Phys. Chem. Chem. Phys.* **2003**, *5*, 4351–4360. [CrossRef]
96. Topsøe, H. Developments in operando studies and in situ characterization of heterogeneous catalysts. *J. Catal.* **2003**, *216*, 155–164. [CrossRef]
97. Grunwaldt, J.D.; Clausen, B.S. Combining XRD and EXAFS with on-line catalytic studies for in situ characterization of catalysts. *Top. Catal.* **2002**, *18*, 37–43. [CrossRef]
98. Banares, M.A. Operando methodology: Combination of in situ spectroscopy and simultaneous activity measurements under catalytic reaction conditions. *Catal. Today* **2005**, *100*, 71–77. [CrossRef]
99. Prakash, A.S.; Shivakumara, C.; Hegde, M.S. Single step preparation of CeO_2/$CeAlO_3$/-Al_2O_3 by solution combustion method: Phase evolution, thermal stability and surface modification. *Mater. Sci. Eng. B* **2007**, *139*, 55–61. [CrossRef]
100. Liang, H.; Zhang, Y.; Liu, Y. Ceria modified three-dimensionally ordered macro-porous Pt/TiO_2 catalysts for water-gas shift reaction. *J. Rare Earth* **2009**, *27*, 425–430. [CrossRef]
101. Laosiripojana, N.; Assabumrungrat, S. Catalytic steam reforming of ethanol over high surface area CeO_2: The role of CeO_2 as an internal pre-reforming catalyst. *Appl. Catal. B Environ.* **2006**, *66*, 29–39. [CrossRef]
102. Yao, H.C.; Yu Yao, Y.F. Ceria in automotive exhaust catalysts: I. Oxygen storage. *J. Catal.* **1984**, *86*, 254–265. [CrossRef]
103. Liu, H.; Zou, X.; Wang, X.; Lu, X.; Ding, W. Effect of CeO_2 addition on Ni/Al_2O_3 catalysts for methanation of carbon dioxide with hydrogen. *J. Nat. Gas Chem.* **2012**, *21*, 703–707. [CrossRef]
104. Rahmani, S.; Rezaei, M.; Meshkani, F. Preparation of promoted nickel catalysts supported on mesoporous nanocrystalline gamma alumina for carbon dioxide methanation reaction. *J. Ind. Eng. Chem.* **2014**, *20*, 4176–4182. [CrossRef]
105. Saha, N.C.; Wolf, E.E. Co methanation activity and XPS studies of Pd supported on ZSM5 and Y-zeolites. *Appl. Catal.* **1984**, *13*, 101–112. [CrossRef]
106. Eckle, S.; Anfang, H.G.; Behm, R.J. Reaction Intermediates and side products in the methanation of CO and CO_2 over supported Ru catalysts in H_2-rich reformate gases. *J. Phys. Chem. C* **2010**, *115*, 1361–1367. [CrossRef]
107. Patzelová, V.; Zukal, A.; Tvarůžková, Z.; Malíček, O. Hydrogenation of CO and CO_2 Over Stabilized NiY Catalysts. *Stud. Surf. Sci. Catal.* **1984**, *18*, 367–374.
108. Graca, I.; González, L.V.; Bacariza, M.C.; Fernandes, A.; Henriques, C.; Lopes, J.M.; Ribeiro, M.F. CO_2 hydrogenation into CH_4 on NiHNaUSY zeolites. *Appl. Catal. B Environ.* **2014**, *147*, 101–110. [CrossRef]
109. Xavier, K.O.; Sreekala, R.; Rashid, K.K.A.; Yusuff, K.K.M.; Sen, B. Doping effects of cerium oxide on Ni/Al_2O_3 catalysts for methanation. *Catal. Today* **1999**, *49*, 17–21. [CrossRef]
110. Rynkowski, J.M.; Paryjczak, T. Characterization of Ru/CeO_2-Al_2O_3 catalysts and their Performance in CO_2 Methanation. *React. Kinet. Catal. Lett.* **2000**, *71*, 55–64. [CrossRef]
111. Westermann, A.; Azambre, B.; Bacariza, M.C.; Graca, I.; Ribeiroa, M.F.; Lopes, J.M.; Henriquesapp, C. Insight into CO_2 methanation mechanism over NiUSY zeolites: An operando IR study. *Appl. Catal. B Environ.* **2015**, *174–175*, 120–125. [CrossRef]
112. Rivero-Mendoza, D.E.; Stanley, J.N.G.; Scott, J.; Aguey-Zinsou, K.F. An alumina-supported Ni-La-based catalyst for producing synthetic natural gas. *Catalysts* **2016**, *6*, 170. [CrossRef]
113. Sokolov, S.; Kondratenko, E.V.; Pohl, M.M.; Barkschat, A.; Rodemerck, U. Stable low-temperature dry reforming of methane over mesoporous La_2O_3-ZrO_2 supported Ni catalyst. *Appl. Catal. B Environ.* **2012**, *113–114*, 19–30. [CrossRef]

114. Rossetti, I.; Biffi, C.; Bianchi, C.L.; Nichele, V.; Signoretto, M.; Menegazzo, F.; Finocchio, E.; Ramis, G.; Di Michele, A. Ni/SiO_2 and Ni/ZrO_2 catalysts for the steam reforming of ethanol. *Appl. Catal. B Environ.* **2012**, *117–118*, 384–396. [CrossRef]
115. Nichele, V.; Signoretto, M.; Menegazzo, F.; Gallo, A.; Dal Santo, V.; Cruciani, G.; Cerrato, G. Glycerol steam reforming for hydrogen production: Design of Ni supported catalysts. *Appl. Catal. B Environ.* **2012**, *111–112*, 225–232. [CrossRef]
116. Zheng, H.; Gao, C.; Peng, B.; Shu, M.; Che, S. pH-Responsive Drug Delivery System Based on Coordination Bonding in a Mesostructured Surfactant/Silica Hybrid. *J. Phys. Chem. C* **2011**, *115*, 7230–7237. [CrossRef]
117. Lin, Y.S.; Haynes, C.L. Impacts of Mesoporous Silica Nanoparticle Size, Pore Ordering, and Pore Integrity on Hemolytic Activity. *J. Am. Chem. Soc.* **2010**, *132*, 4834–4842. [CrossRef] [PubMed]
118. Liong, M.; Angelos, S.; Choi, E.; Patel, K.; Fraser Stoddart, J.; Zink, J.I. Mesostructured multifunctional nanoparticles for imaging and drug delivery. *J. Mater. Chem.* **2009**, *19*, 6251–6257. [CrossRef]
119. Sakamoto, Y.; Kaneda, M.; Terasaki, O.; Zhao, D.Y.; Kim, J.M.; Stucky, G.; Shin, H.J.; Ryoo, R. Direct imaging of the pores and cages of three-dimensional mesoporous materials. *Nature* **2000**, *408*, 449–453. [PubMed]
120. Dou, J.; Zeng, H.C. Targeted Synthesis of Silicomolybdic Acid (Keggin Acid) inside Mesoporous Silica Hollow Spheres for Friedel–Crafts Alkylation. *J. Am. Chem. Soc.* **2012**, *134*, 16235–16246. [CrossRef] [PubMed]
121. Jiao, F.; Frei, H. Nanostructured Cobalt Oxide Clusters in Mesoporous Silica as Efficient Oxygen-Evolving Catalysts. *Angew. Chem. Int. Ed.* **2009**, *48*, 1841–1844. [CrossRef] [PubMed]
122. Hulea, V.; Brunel, D.; Galarneau, A.; Philippot, K.; Chaudret, B.; Kooyman, P.J.; Fajula, F. Synthesis of well-dispersed ruthenium nanoparticles inside mesostructured porous silica under mild conditions. *Microporous Mesoporous Mater.* **2005**, *79*, 185–194. [CrossRef]
123. Aziz, M.A.A.; Jalil, A.A.; Triwahyono, S.; Mukti, R.R.; Taufiq-Yap, Y.H.; Sazegar, M.R. Highly active Ni-promoted mesostructured silica nanoparticles for CO_2 methanation. *Appl. Catal. B Environ.* **2014**, *147*, 359–368. [CrossRef]
124. Aziz, M.A.A.; Jalil, A.A.; Triwahyono, S.; Sidik, S.M. Methanation of carbon dioxide on metal-promoted mesostructured silica nanoparticles. *Appl. Catal. A Gen.* **2014**, *486*, 115–122. [CrossRef]
125. Aziz, M.A.A.; Jalil, A.A.; Triwahyono, S.; Saad, M.W.A. CO_2 methanation over Ni-promoted mesostructured silica nanoparticles: Influence of Ni loading and water vapor on activity and response surface methodology studies. *Chem. Eng. J.* **2015**, *260*, 757–764. [CrossRef]
126. Du, G.; Lim, S.; Yang, Y.; Wang, C.; Pfefferle, L.; Haller, G.L. Methanation of carbon dioxide on Ni-incorporated MCM-41 catalysts: The influence of catalyst pretreatment and study of steady-state reaction. *J. Catal.* **2007**, *249*, 370–379. [CrossRef]
127. Pan, Q.; Peng, J.; Wang, S.; Wang, S. In situ FTIR spectroscopic study of the CO_2 methanation mechanism on Ni/$Ce_{0.5}Zr_{0.5}O_2$. *Catal. Sci. Technol.* **2014**, *4*, 502–509. [CrossRef]
128. Fujita, S.I.; Nakamura, M.; Doi, T.; Takezawa, N. Mechanisms of methanation of carbon dioxide and carbon monoxide over nickel/alumina catalysts. *Appl. Catal. A Gen.* **1993**, *104*, 87–100. [CrossRef]
129. Kwak, J.H.; Kovarik, L.; Szanyi, J. CO_2 Reduction on Supported Ru/Al_2O_3 Catalysts: Cluster Size Dependence of Product Selectivity. *ACS Catal.* **2013**, *3*, 2449–2455. [CrossRef]
130. Benítez, J.J.; Alvero, R.; Capitán, M.J.; Carrizosa, I.; Odriozola, J.A. DRIFTS study of adsorbed formate species in the carbon dioxide and hydrogen reaction over rhodium catalysts. *Appl. Catal.* **1991**, *71*, 219–231. [CrossRef]
131. Dalla Betta, R.A.; Shelef, M. Heterogeneous methanation: In situ infrared spectroscopic study of $RuAl_2O_3$ during the hydrogenation of CO. *J. Catal.* **1977**, *48*, 111–119. [CrossRef]
132. Bartholomew, C.H.; Pannell, R.B.; Fowler, R.W. Sintering of alumina-supported nickel and nickel bimetallic methanation catalysts in H_2H_2O atmospheres. *J. Catal.* **1983**, *79*, 34–46. [CrossRef]
133. Zhang, J.; Xin, Z.; Meng, X.; Tao, M. Synthesis, characterization and properties of anti-sintering nickel incorporated MCM-41 methanation catalysts. *Fuel* **2013**, *109*, 693–701. [CrossRef]
134. Huber, G.W.; Iborra, S.; Corma, A. Synthesis of Transportation Fuels from Biomass: Chemistry, Catalysts and Engineering. *Chem. Rev.* **2006**, *106*, 4044–4098. [CrossRef] [PubMed]
135. Yung, M.M.; Jablonski, W.S.; Magrini-Bair, K.A. Review of Catalytic Conditioning of Biomass-Derived Syngas. *Energy Fuels* **2009**, *23*, 1874–1887. [CrossRef]

136. Zhao, D.; Feng, J.; Huo, Q.; Melosh, N.; Fredrickson, G.H.; Chmelka, B.F.; Stucky, G.D. Triblock Copolymer Syntheses of Mesoporous Silica with Periodic 50 to 300 Angstrom Pores. *Science* **1998**, *279*, 548–552. [CrossRef] [PubMed]
137. Zhao, D.; Huo, Q.; Feng, J.; Chmelka, B.F.; Stucky, G.D. Nonionic Triblock and Star Diblock Copolymer and Oligomeric Surfactant Syntheses of Highly Ordered, Hydrothermally Stable, Mesoporous Silica Structures. *J. Am. Chem. Soc.* **1998**, *120*, 6024–6036. [CrossRef]
138. Cheng, M.Y.; Pan, C.J.; Hwang, B.J. Highly-dispersed and thermally-stable NiO nanoparticles exclusively confined in SBA-15: Blockage-free nanochannels. *J. Mater. Chem.* **2009**, *19*, 5193–5200. [CrossRef]
139. Vradman, L.; Landau, M.V.; Kantorovich, D.; Koltypin, Y.; Gedanken, A. Evaluation of metal oxide phase assembling mode inside the nanotubular pores of mesostructured silica. *Microporous Mesoporous Mater.* **2005**, *79*, 307–318. [CrossRef]
140. Lu, B.; Kawamoto, K. Preparation of the highly loaded and well-dispersed NiO/SBA-15 for methanation of producer gas. *Fuel* **2013**, *103*, 699–704. [CrossRef]
141. Köck, E.M.; Kogler, M.; Bielz, T.; Klötzer, B.; Penner, S. In Situ FT-IR Spectroscopic Study of CO_2 and CO Adsorption on Y_2O_3, ZrO_2, and Yttria-Stabilized ZrO_2. *J. Phys. Chem. C* **2013**, *117*, 17666–17673. [CrossRef] [PubMed]
142. Pokrovski, K.; Jung, K.T.; Bell, A.T. Investigation of CO and CO_2 adsorption on tetragonal and monoclinic zirconia. *Langmuir* **2001**, *17*, 4297–4303. [CrossRef]
143. Baeza, B.B.; Ramos, I.R.; Ruiz, A.G. Interaction of Carbon Dioxide with the Surface of Zirconia Polymorphs. *Langmuir* **1998**, *14*, 3556–3564. [CrossRef]
144. Yamasaki, M.; Habazaki, H.; Yoshida, T.; Akiyama, E.; Kawashima, A.; Asami, K.; Hashimoto, K.; Komori, M.; Shimamura, K. Compositional dependence of the CO_2 methanation activity of Ni/ZrO_2 catalysts prepared from amorphous Ni-Zr alloy precursors. *Appl. Catal. A Gen.* **1997**, *163*, 187–197. [CrossRef]
145. Habazaki, H.; Tada, T.; Wakuda, K.; Kawashima, A.; Asami, K.; Hashimoto, K. *Corrosion, Electrochemistry and Catalysis of Metastable Metals and Intermetallics*; Clayton, C.R., Hashimoto, K., Eds.; The Electrochemical Society: Washington, DC, USA, 1993; p. 393.
146. Yamasaki, M.; Habazaki, H.; Asami, K.; Izumiya, K.; Hashimoto, K. Effect of tetragonal ZrO_2 on the catalytic activity of Ni/ZrO_2 catalyst prepared from amorphous Ni-Zr alloys. *Catal. Commun.* **2006**, *7*, 24–28. [CrossRef]
147. Yamasaki, M.; Komori, M.; Akiyama, E.; Habazaki, H.; Kawashima, A.; Asami, K.; Hashimoto, K. CO_2 methanation catalysts prepared from amorphous Ni-Zr-Sm and Ni-Zr-misch metal alloy precursors. *Mater. Sci. Eng. A* **1999**, *267*, 220–226. [CrossRef]
148. Habazaki, H.; Yamasaki, M.; Kawashima, A.; Hashimoto, K. Methanation of carbon dioxide on $Ni/(Zr\text{-}Sm)O_x$ catalysts. *Appl. Organomet. Chem.* **2000**, *14*, 803–808. [CrossRef]
149. Huang, Y.H.; Wang, J.J.; Liu, Z.M.; Lin, G.D.; Zhang, H.B. Highly efficient Ni-ZrO_2 catalyst doped with Yb_2O_3 for co-methanation of CO and CO_2. *Appl. Catal. A Gen.* **2013**, *466*, 300–306. [CrossRef]
150. Takano, H.; Izumiyaa, K.; Kumagai, N.; Hashimoto, K. The effect of heat treatment on the performance of the Ni/(Zr-Sm oxide) catalysts for carbon dioxide methanation. *Appl. Surf. Sci.* **2011**, *257*, 8171–8176. [CrossRef]
151. Qin, Z.; Ren, J.; Miao, M.; Li, Z.; Lin, J.; Xie, K. The catalytic methanation of coke oven gas over $Ni\text{-}Ce/Al_2O_3$ catalyst prepared by microwave heating: Effect of amorphous NiO formation. *Appl. Catal. B* **2015**, *164*, 18–30. [CrossRef]
152. Zhou, G.; Liu, H.; Cui, K.; Jia, A.; Hu, G.; Jiao, Z.; Liu, Y.; Zhang, X. Role of surface Ni and Ce species of Ni/CeO_2 catalyst in CO_2 methanation. *Appl. Surf. Sci.* **2016**, *383*, 248–252. [CrossRef]
153. Konishcheva, M.V.; Potemkin, D.I.; Badmaev, S.D.; Snytnikov, P.V.; Paukshtis, E.A.; Sobyanin, V.A.; Parmon, V.N. On the mechanism of CO and CO_2 methanation over Ni/CeO_2 catalysts. *Top. Catal.* **2016**, *59*, 1424–1430. [CrossRef]
154. Nematollahi, B.; Rezaei, M.; Nemati Lay, E. Selective methanation of carbon monoxide in hydrogen rich stream over Ni/CeO_2 nanocatalysts. *J. Rare Earth* **2015**, *33*, 619–628. [CrossRef]
155. Ocampo, F.; Louis, B.; Roger, A.C. Methanation of carbon dioxide over nickel-based $Ce_{0.72}Zr_{0.28}O_2$ mixed oxide catalysts prepared by sol–gel method. *Appl. Catal. A Gen.* **2009**, *369*, 90–96. [CrossRef]
156. Laosiripojana, N.; Assabumrungrat, S. Methane steam reforming over $Ni/Ce\text{–}ZrO_2$ catalyst: Influences of $Ce\text{-}ZrO_2$ support on reactivity, resistance toward carbon formation and intrinsic reaction kinetics. *Appl. Catal. A Gen.* **2005**, *290*, 200–211. [CrossRef]

157. Di Monte, R.; Fornasiero, P.; Kašpar, J.; Rumori, P.; Gubitosa, G.; Graziani, M. $Pd/Ce_{0.6}Zr_{0.4}O_2/Al_2O_3$ as advanced materials for three-way catalysts Part 1. Catalyst characterisation, thermal stability and catalytic activity in the reduction of NO by CO. *Appl. Catal. B Environ.* **2000**, *24*, 157–167. [CrossRef]
158. Strobel, R.; Krumeich, F.; Pratsinis, S.E.; Baiker, A. Flame-derived $Pt/Ba/Ce_xZr_{1-x}O_2$: Influence of support on thermal deterioration and behavior as NO_x storage-reduction catalysts. *J. Catal.* **2006**, *243*, 229–238. [CrossRef]
159. Ocampo, F.; Louis, B.; Kiwi-Minsker, L.; Roger, A.C. Effect of Ce/Zr composition and noble metal promotion on nickel based $Ce_xZr_{1-x}O_2$ catalysts for carbon dioxide methanation. *Appl. Catal. A Gen.* **2011**, *392*, 36–44. [CrossRef]
160. Haneda, M.; Shinoda, K.; Nagane, A.; Houshito, O.; Takagi, H.; Nakahara, Y.; Hiroe, K.; Fujitani, T.; Hamada, H. Catalytic performance of rhodium supported on ceria–zirconia mixed oxides for reduction of NO by propene. *J. Catal.* **2008**, *259*, 223–231. [CrossRef]
161. Silva, P.P.; Silva, F.A.; Portela, L.S.; Mattos, L.V.; Noronha, F.B.; Hori, C.E. Effect of Ce/Zr ratio on the performance of $Pt/CeZrO_2/Al_2O_3$ catalysts for methane partial oxidation. *Catal. Today* **2005**, *107–108*, 734–740. [CrossRef]
162. Koubaissy, B.; Pietraszek, A.; Roger, A.C.; Kiennemann, A. CO_2 reforming of methane over Ce-Zr-Ni-Me mixed catalysts. *Catal. Today* **2010**, *157*, 436–439. [CrossRef]
163. Youn, M.H.; Gil Seo, J.; Min Cho, K.; Park, S.; Park, D.R.; Jung, J.C.; Song, I.K. Hydrogen production by auto-thermal reforming of ethanol over nickel catalysts supported on Ce-modified mesoporous zirconia: Effect of Ce/Zr molar ratio. *Int. J. Hydrogen Energy* **2008**, *33*, 5052–5059. [CrossRef]
164. Ussa Aldana, P.A.; Ocampo, F.; Kobl, K.; Louis, B.; Thibault-Starzyka, F.; Daturi, M.; Bazina, P.; Thomas, S.; Roger, A.C. Catalytic CO_2 valorization into CH_4 on Ni-based ceria-zirconia. Reaction mechanism by operando IR spectroscopy. *Catal. Today* **2013**, *215*, 201–207. [CrossRef]
165. Pan, Q.; Peng, J.; Sun, T.; Wang, S.; Wang, S. Insight into the reaction route of CO_2 methanation: Promotion effect of medium basic sites. *Catal. Commun.* **2014**, *45*, 74–78. [CrossRef]
166. Korhonen, S.T.; Calatayud, M.; Krause, A.O.I. Structure and Stability of Formates and Carbonates on Monoclinic Zirconia: A Combined Study by Density Functional Theory and Infrared Spectroscopy. *J. Phys. Chem. C* **2008**, *112*, 16096–16102. [CrossRef]
167. Nizio, M.; Albarazi, A.; Cavadias, S.; Amouroux, J.; Galvez, M.E.; Da Costa, P. Hybrid plasma-catalytic methanation of CO_2 at low temperature over ceria zirconia supported Ni catalysts. *Int. J. Hydrogen Energy* **2016**, *41*, 11584–11592. [CrossRef]
168. Li, C.; Sakata, Y.; Arai, T.; Domen, K.; Maruya, K.; Onishi, T. Carbon monoxide and carbon dioxide adsorption on cerium oxide studied by Fourier-transform infrared spectroscopy. Part 1.Formation of carbonate species on dehydroxylated CeO_2, at room temperature. *J. Chem. Soc. Faraday Trans.* **1989**, *85*, 929–943. [CrossRef]
169. Jin, T.; Zhou, Y.; Mains, G.J.; White, J.M. Infrared and X-ray Photoelectron Spectroscopy Study of CO and CO_2 on Pt/CeO_2. *J. Phys. Chem.* **1987**, *91*, 5931–5937. [CrossRef]
170. Marwood, M.; Doepper, R.; Renken, A. In-situ surface and gas phase analysis for kinetic studies under transient conditions the catalytic hydrogenation of CO_2. *Appl. Catal. A Gen.* **1997**, *151*, 223–246. [CrossRef]
171. Prairie, M.R.; Highfield, J.G.; Renken, A. Diffuse-reflectance FTIR spectroscopy for kinetic and mechanistic studies of CO_2 hydrogenation in a continuous recycle reactor. *Chem. Eng. Sci.* **1991**, *46*, 113–121. [CrossRef]
172. Prairie, M.R.; Renken, A.; Highfield, J.G.; Ravindranathan Thampi, K.; Grätzel, M. A Fourier transform infrared spectroscopic study of CO_2 methanation on supported ruthenium. *J. Catal.* **1991**, *129*, 130–144. [CrossRef]
173. Schild, C.; Wokaun, A. CO_2 hydrogenation over Nickel/Zirconia catalysts from amorphous precursors: On the mechanism of methane formation. *J. Phys. Chem.* **1991**, *95*, 6341–6346. [CrossRef]
174. Schild, C.; Wokaun, A.; Baiker, A. Surface species in CO_2 methanation over amorphous palladium/zirconia catalysts. *J. Mol. Catal.* **1991**, *69*, 347–357. [CrossRef]
175. Benitez, J.J.; Carrizosa, I.; Odriozola, J.A. HCOOH hydrogenation over lanthanide-oxide-promoted Rh/Al_2O_3 catalysts. *Appl. Surf.* **1993**, *68*, 565–573. [CrossRef]
176. Yashima, M.; Morimoto, K.; Ishizawa, N.; Yoshimura, M. Diffusionless Tetragonal–Cubic Transformation Temperature in Zirconia–Ceria Solid Solutions. *J. Am. Ceram. Soc.* **1993**, *76*, 2865–2868. [CrossRef]

177. Yashima, M.; Morimoto, K.; Ishizawa, N.; Yoshimura, M. Zirconia–Ceria Solid Solution Synthesis and the Temperature–Time–Transformation Diagram for the 1:1 Composition. *J. Am. Chem. Soc.* **1993**, *76*, 1745–1750. [CrossRef]
178. Yashima, M.; Ohtake, K.; Arashi, H.; Kakihana, M.; Yoshimura, M. Determination of cubic-tetragonal phase boundary in $Zr_{1-x}Y_xO_{2-x/2}$ solid solutions by Raman spectroscopy. *J. Appl. Phys.* **1993**, *74*, 7603–7605. [CrossRef]
179. Yashima, M.; Arashi, H.; Kakihana, M.; Yoshimura, M. Raman Scattering Study of Cubic–Tetragonal Phase Transition in $Zr_{1-x}Ce_xO_2$ Solid Solution. *J. Am. Ceram. Soc.* **1994**, *77*, 1067–1071. [CrossRef]
180. Pan, Q.; Peng, J.; Sun, T.; Gao, D.; Wang, S.; Wang, S. CO_2 methanation on $Ni/Ce_{0.5}Zr_{0.5}O_2$ catalysts for the production of synthetic natural gas. *Fuel Proc. Technol.* **2014**, *123*, 166–171. [CrossRef]
181. Kozlov, A.I.; Kim, D.H.; Yezerets, A.; Andersen, P.; Kung, H.H.; Kung, M.C. Effect of Preparation Method and Redox Treatment on the Reducibility, and Structure of Supported Ceria-Zirconia Mixed Oxide. *J. Catal.* **2002**, *209*, 417–426. [CrossRef]
182. Wang, L.; Zhang, S.; Liu, Y. Reverse water gas shift reaction over Co-precipitated Ni-CeO_2 catalysts. *J. Rare Earth* **2008**, *26*, 66–70. [CrossRef]
183. Roh, H.S.; Potdar, H.S.; Jun, K.W.; Kim, J.W.; Oh, Y.S. Carbon dioxide reforming of methane over Ni incorporated into Ce-ZrO_2 catalysts. *Appl. Catal. A* **2004**, *276*, 231–239. [CrossRef]
184. Takano, H.; Shinomiya, H.; Izumiya, K.; Kumagai, N.; Habazaki, H.; Hashimoto, K. CO_2 methanation of Ni catalysts supported on tetragonal ZrO_2 doped with Ca^{2+} and Ni^{2+} ions. *Int. J. Hydrogen Energy* **2015**, *40*, 8347–8355. [CrossRef]
185. Perkas, N.; Amirian, G.; Zhong, Z.; Teo, J.; Gofer, Y.; Gedanken, A. Methanation of Carbon Dioxide on Ni Catalysts on Mesoporous ZrO_2 Doped with Rare Earth Oxides. *Catal. Lett.* **2009**, *130*, 455–462. [CrossRef]
186. Cai, M.; Wen, J.; Chu, W.; Cheng, X.; Li, Z. Methanation of carbon dioxide on Ni/ZrO_2-Al_2O_3 catalysts: Effects of ZrO_2 promoter and preparation method of novel ZrO_2-Al_2O_3 carrier. *J. Nat. Gas Chem.* **2011**, *20*, 318–324. [CrossRef]
187. Lu, H.; Yang, X.; Gao, G.; Wang, K.; Shi, Q.; Wang, J.; Han, C.; Liu, J.; Tong, M.; Liang, X.; et al. Mesoporous zirconia-modified clays supported nickel catalysts for CO and CO_2 methanation. *Int. J. Hydrogen Energy* **2014**, *39*, 18894–18907. [CrossRef]
188. Abate, S.; Mebrahtu, C.; Giglio, E.; Deorsola, F.; Bensaid, S.; Perathoner, S.; Pirone, R.; Centi, G. Catalytic performance of γ-Al_2O_3-ZrO_2-TiO_2-CeO_2 composite oxide supported Ni-based catalysts for CO_2 methanation. *Int. Eng. Chem. Res.* **2016**, *55*, 4451–4460. [CrossRef]
189. Zhang, J.; Xu, Y.F.; Qian, G.; Xu, Z.P.; Chen, C.; Liu, Q. Reinvestigation of dehydration and dehydroxylation of hydrotalcite-like compounds through combined TG-DTA-MS analyses. *J. Phys. Chem.* **2010**, *114*, 10768–10774. [CrossRef]
190. Abate, S.; Barbera, K.; Giglio, E.; Deorsola, F.; Bensaid, S.; Perathoner, S.; Pirone, R.; Centi, G. Synthesis, characterization and activity pattern of Ni-Al Hydrotalcite catalysts in CO_2 methanation. *Ind. Eng. Chem. Res.* **2016**, *55*, 8299–8308. [CrossRef]
191. He, L.; Lin, Q.; Liu, Y.; Huang, Y. Unique catalysis of Ni-Al hydrotalcite derived catalyst in CO_2 methanation: Cooperative effect between Ni nanoparticle and a basic support. *J. Energy Chem.* **2014**, *23*, 587–592. [CrossRef]
192. Gabrovska, M.; Edreva-Kardjieva, R.; Crisan, D.; Tzvetkov, P.; Shopska, M.; Shtereva, I. Ni-Al layered double hydroxides as catalyst precursors for CO_2 removal by methanation. *React. Kinet. Mech. Catal.* **2012**, *105*, 79–99. [CrossRef]
193. Wierzbicki, D.; Debek, R.; Motak, M.; Grzybek, T.; Galvez, M.E.; Da Costa, P. Novel Ni-La-hydrotalcite derived catalysts for CO_2 methanation. *Catal. Commun.* **2016**, *83*, 5–8. [CrossRef]
194. Feng, Y.; Yang, W.; Chen, S.; Chu, W. Cerium promoted nano nickel catalysts Ni-Ce/CNTs and Ni-Ce/Al_2O_3 for CO_2 methanation. *Integr. Ferroelectr.* **2014**, *151*, 116–125. [CrossRef]
195. Yan, Y.; Dai, Y.; He, H.; Yu, Y.; Yang, Y. A novel W-doped Ni-Mg mixed oxide catalysts for CO_2 methanation. *Appl. Catal. B Environ.* **2016**, *196*, 108–116. [CrossRef]
196. Merkache, R.; Fechete, I.; Maamache, M.; Bernard, M.; Turek, P.; Al-Dalama, K.; Garin, F. 3D ordered mesoporous Fe-KIT-6 catalysts for methylcyclopentane (MCP) conversion and carbon dioxide (CO_2) hydrogeneation for energy and environmental applications. *Appl. Catal. A Gen.* **2015**, *504*, 672–681. [CrossRef]
197. Tsuji, M.; Kodama, T.; Yoshida, T.; Kitayama, Y.; Tamaura, Y. Preparation and CO_2 Methanation Activity of an ultrafine Ni(II) Ferrite Catalyst. *J. Catal.* **1996**, *164*, 315–321. [CrossRef]

198. Nishizawa, K.; Kodama, T.; Tabata, M.; Yoshida, T.; Tsuji, M.; Tamaura, Y. Adsorption of CO_2 on oxygen-deficient magnetite: Adsorption enthalpy and adsorption isotherm. *J. Chem. Soc. Faraday Trans.* **1992**, *88*, 2771–2773. [CrossRef]
199. Yoshida, T.; Nishizawa, K.; Tabata, M.; Abe, H.; Kodama, T.; Tsuji, M.; Tamaura, Y. Methanation of CO_2 with H_2-reduced magnetite. *J. Mater. Sci.* **1993**, *28*, 1220–1226. [CrossRef]
200. Nishizawa, K.; Kato, H.; Mimori, K.; Yoshida, T.; Hasegawa, N.; Tsuji, M.; Tamaura, Y. Methanation of carbon deposited directly from CO_2 on rhodium-bearing activated magnetite. *J. Mater. Sci.* **1994**, *29*, 768–772. [CrossRef]
201. Tsuji, M.; Nishizawa, K.; Yoshida, T.; Tamaura, Y. Methanation reactivity of carbon deposited directly from CO_2 on to the oxygen-deficient magnetite. *J. Mater. Sci.* **1994**, *29*, 5481–5484. [CrossRef]
202. Tsuji, M.; Kato, H.; Kodama, T.; Chang, S.G.; Hesegawa, N.; Tamaura, Y. Methanation of CO_2 on H_2-reduced Ni(II)-or Co(II)-bearing ferrites at 200 °C. *J. Mater. Sci.* **1994**, *29*, 6227–6230. [CrossRef]
203. Kato, H.; Sano, T.; Wada, Y.; Tamaura, Y.; Tsuji, M.; Tsuji, T.; Miyazaki, S. Methanation of CO_2 with the oxygen-deficient Ni(II)-ferrite under dynamic conditions. *J. Mater. Sci.* **1995**, *30*, 6350–6354. [CrossRef]
204. Kodama, T.; Kitayama, Y.; Tsuji, M.; Tamaura, Y. Methanation of CO_2 using ultrafine $Ni_xFe_{3-x}O_4$. *Energy* **1997**, *22*, 183–187. [CrossRef]
205. Yoshida, T.; Tsuji, M.; Tamaura, Y.; Hurue, T.; Hayashida, T.; Ogawa, K. Carbon recycling system through methanation of CO_2 in flue gas in LNG power plant. *Energy Convers. Manag.* **1997**, *38*, 443–448. [CrossRef]
206. Bligaard, T.; Nørskov, J.K.; Dahl, S.; Matthiesen, J.; Christensen, C.H.; Sehested, J. The Brønsted–Evans–Polanyi relation and the volcano curve in heterogeneous catalysis. *J. Catal.* **2004**, *224*, 206–217. [CrossRef]
207. Andersson, M.P.; Bligaard, T.; Kustov, A.; Larsen, K.E.; Greeley, J.; Johannessen, T.; Christensen, C.H.; Nørskov, J.K. Toward computational screening in heterogeneous catalysis: Pareto-optimal methanation catalysts. *J. Catal.* **2006**, *239*, 501–506. [CrossRef]
208. Sehesteda, J.; Larsen, K.E.; Kustov, A.L.; Frey, A.M.; Johannessen, T.; Bligaard, T.; Andersson, M.P.; Nørskov, J.K.; Christensen, C.H. Discovery of technical methanation catalysts based on computational Screening. *Top. Catal.* **2007**, *45*, 9–13. [CrossRef]
209. Kustov, A.L.; Frey, A.M.; Larsen, K.E.; Johannessen, T.; Nørskov, J.K.; Christensen, C.H. CO methanation over supported bimetallic Ni-Fe catalysts: From computational studies towards catalyst optimization. *Appl. Catal. A Gen.* **2007**, *320*, 98–104. [CrossRef]
210. Ertl, G.; Knozinger, H.; Schüth, F.; Weitkamp, J. *Handbook of Heterogenous Catalysis*; Wiley-VCH: Weinheim, Germany, 1997.
211. Dumesic, J.A.; Rudd, D.F.; Aparicio, L.M.; Rekoske, J.E.; Treviño, A.A. *The Microkinetics of Heterogeneous Catalysis*; ACS Professional Reference Book; American Chemical Society: Washington, DC, USA, 1993; p. 315.
212. Boudart, M.; Djega-Mariadassou, G. *Kinetics of Heterogeneous Catalytic Reactions*; Pricenton University: Princeton, NJ, USA, 1984.
213. Nørskov, J.K.; Bligaard, T.; Logadottir, A.; Bahn, S.; Hansen, L.B.; Bollinger, M.; Bengaard, H.; Hammer, B.; Sljivancanin, Z.; Mavrikakis, M.; et al. Universality in Heterogeneous Catalysis. *J. Catal.* **2002**, *209*, 275–278. [CrossRef]
214. Linic, S.; Barteau, M.A. Control of Ethylene Epoxidation Selectivity by Surface Oxametallacycles. *J. Am. Chem. Soc.* **2003**, *125*, 4034–4035. [CrossRef] [PubMed]
215. Reuter, K.; Frenkel, D.; Scheffler, M. The Steady State of Heterogeneous Catalysis, Studied by First-Principles Statistical Mechanics. *Phys. Rev. Lett.* **2004**, *93*, 116105. [CrossRef] [PubMed]
216. Honkala, K.; Hellman, A.; Remediakis, I.N.; Logadottir, A.; Carlsson, A.; Dahl, S.; Christensen, C.H.; Nørskov, J.K. Ammonia Synthesis from First-Principles Calculations. *Science* **2005**, *307*, 555–558. [CrossRef] [PubMed]
217. Pareto, V.; Montesano, A.; Zanni, A.; Bruni, L.; Chipman, J.S.; McLure, M. *Manual of Political Economy: A Critical and Variorum Edition*, 1st ed.; Oxford University Press: Oxford, UK, 2014.
218. Bligaard, T.; Jóhannesson, G.H.; Ruban, A.V.; Skriver, H.L.; Jacobsen, K.W.; Nørskov, J.K. Pareto-optimal alloys. *Appl. Phys. Lett.* **2003**, *83*, 4527–4529. [CrossRef]
219. Mori, S.; Xu, W.C.; Ishidzuki, T.; Ogasawara, N.; Imai, J.; Kobayashi, K. Mechanochemical activation of catalysts for CO_2 methanation. *Appl. Catal. A Gen.* **1996**, *137*, 255–268. [CrossRef]

220. Yaccato, K.; Carhart, R.; Hagemeyer, A.; Lesik, A.; Strasser, P.; Volpe, A.F., Jr.; Turner, H.; Weinberg, H.; Grasselli, R.K.; Brooks, C. Competitive CO and CO_2 methanation over supported noble metal catalysts in high throughput scanning mass spectrometer. *Appl. Catal. A Gen.* **2005**, *296*, 30–48. [CrossRef]
221. Ren, J.; Guo, H.; Yang, J.; Qin, Z.; Lin, J.; Li, Z. Insights into the mechanisms of CO_2 methanation on Ni(111) surfaces by density functional theory. *Appl. Surf. Sci.* **2015**, *351*, 504–516. [CrossRef]
222. Goodman, D.J. Methanation of Carbon Dioxide. Mc.S. Thesis, University of California, Los Angeles, CA, USA, 2013; pp. 1–38.
223. Lapidus, A.L.; Gaidai, N.A.; Nekrasov, N.V.; Tishkova, L.A.; Agafonov, Y.A.; Myshenkova, T.N. The mechanism of carbon dioxide hydrogenation on copper and nickel catalysts. *Pet. Chem.* **2007**, *47*, 75–82. [CrossRef]
224. Miao, B.; Ma, S.S.K.; Wang, X.; Su, H.; Chan, S.H. Catalysis mechanism of CO_2 and CO methanation. *Catal. Sci. Technol.* **2016**, *6*, 4048–4058. [CrossRef]
225. Choe, S.J.; Kang, H.J.; Kim, S.J.; Park, S.B.; Park, D.H.; Huh, D.S. Adsorbed carbon formation and carbon hydrogenation for CO_2 methanation on the Ni(111) surface: ASED-MO study. *Bull. Korean Chem. Soc.* **2005**, *26*, 1682–1688.
226. Panagiotopoulou, P.; Kondarides, D.I.; Verykios, X.E. Mechanistic aspects of the selective methanation of CO over Ru/TiO_2 catalyst. *Catal. Today* **2012**, *181*, 138–147. [CrossRef]
227. Medsforth, S. CLXIX—Promotion of catalytic reactions: Part I. *J. Chem. Soc. Trans.* **1923**, *123*, 1452–1469. [CrossRef]
228. Schild, C.; Wokaun, A.; Baiker, A. On the mechanism of CO and CO_2 hydrogenation reactions on zirconia-supported catalysts: A diffuse reflectance FTIR study: Part II. Surface species on copper/zirconia catalysts: Implications for methanoi synthesis selectivity. *J. Mol. Catal.* **1990**, *63*, 243–255. [CrossRef]
229. Kang, S.H.; Ryu, J.H.; Kim, J.H.; Seo, S.J.; Yoo, Y.D.; Prasad, P.S.S.; Lim, H.J.; Byun, C.D. Co-methanation of CO and CO_2 on the Ni_x-Fe_{1-x}/Al_2O_3 catalysts: Effect of Fe contents. *Korean J. Chem. Eng.* **2011**, *28*, 2282–2286. [CrossRef]
230. Hwang, S.; Lee, J.; Hong, U.G.; Jung, J.C.; Koh, D.J.; Lim, H.; Byun, C.; Song, I.K. Hydrogenation of carbon monoxide to methane over mesoporous nickel-M-alumina (M = Fe, Ni, Co, Ce, and La) xerogel catalysts. *Ind. Eng. Chem.* **2012**, *18*, 243–248. [CrossRef]
231. Hwang, S.; Hong, U.G.; Lee, J.; Seo, J.G.; Baik, J.H.; Koh, D.J.; Lim, H.; Song, I.K. Methanation of carbon dioxide over mesoporous Ni-Fe-Al_2O_3 catalysts prepared by a coprecipitation method: Effect of precipitation agent. *Ind. Eng. Chem.* **2013**, *19*, 2016–2021. [CrossRef]
232. Hwang, S.; Lee, J.; Hong, U.G.; Baik, J.H.; Koh, D.J.; Lim, H.; Song, I.K.S. Methanation of carbon dioxide over mesoporous Ni-Fe-Ru-Al_2O_3 xerogel catalysts: Effect of ruthenium content. *Ind. Eng. Chem.* **2013**, *19*, 698–703. [CrossRef]
233. Kopyscinski, J.; Schildhauer, T.J.; Biollaz, S.M.A. Employing Catalyst Fluidization to Enable Carbon Management in the Synthetic Natural Gas Production from Biomass. *Chem. Eng. Technol.* **2009**, *32*, 343–347. [CrossRef]
234. Panagiotopoulou, P.; Kondarides, D.I.; Verykios, X.E. Selective methanation of CO over supported Ru catalysts. *Appl. Catal. B Environ.* **2009**, *88*, 470–478. [CrossRef]
235. Park, E.D.; Lee, D.; Lee, H.C. Recent progress in selective CO removal in a H_2-rich stream. *Catal. Today* **2009**, *139*, 280–290. [CrossRef]
236. Snel, R. Supported iron catalysts in Fischer-Tropsch synthesis: Influence of the preparation method. *Ind. Eng. Chem. Res.* **1989**, *28*, 654–659. [CrossRef]
237. Tsuji, M.; Wada, Y.; Yamamoto, T.; Sano, T.; Tamaura, Y. CO_2 decomposition by metallic phase on oxygen-deficient Ni(II)-bearing ferrite. *J. Mater. Sci. Lett.* **1996**, *15*, 156–158. [CrossRef]
238. Choung, J.W.; Xu, Z. Role of complexing agents in ferrite formation under ambient conditions. *Ind. Eng. Chem. Res.* **1999**, *38*, 4689–4693. [CrossRef]
239. Rondinone, A.J.; Samia, A.C.S.; Zhang, Z.J. A chemometric approach for predicting the size of magnetic spinel ferrite nanoparticles from the synthesis conditions. *J. Phys. Chem. B* **2000**, *104*, 7919–7922. [CrossRef]
240. Luo, H.Y.; Yue, Z.X.; Zhou, J. Synthesis and high-frequency magnetic properties of sol-gel derived Ni-Zn ferrite forsterite composites. *J. Magn. Magn. Mater.* **2000**, *210*, 104–108. [CrossRef]
241. Tamaura, Y.; Tahata, M. Complete reduction of carbon dioxide to carbon using cation-excess magnetite. *Nature* **1990**, *346*, 255–256. [CrossRef]

242. Kato, H.; Kodama, T.; Tsuji, M.; Tamaura, Y. Decomposition of carbon dioxide to carbon by hydrogen-reduced Ni(II)-bearing ferrite. *J. Mater. Sci.* **1994**, *29*, 5689–5692. [CrossRef]
243. Tabata, M.; Nishida, Y.; Kodama, T.; Mimori, K.; Yoshida, T.; Tamaura, Y. CO_2 decomposition with oxygen-deficient Mn(II) ferrite. *J. Mater. Sci.* **1993**, *28*, 971–974. [CrossRef]
244. Tabata, M.; Akanuma, K.; Nishizawa, K.; Mimori, K.; Yoshida, T.; Tsuji, M.; Tamaura, Y. Reactivity of oxygen-deficient Mn(II)-bearing ferrites ($Mn_xFe_{3-x}O_{4-\delta}$, $0 \leq x \geq \delta > 0$) toward CO_2 decomposition to carbon. *J. Mater. Sci.* **1993**, *28*, 6753–6760. [CrossRef]
245. Kodama, T.; Tabata, M.; Sano, T.; Tsuji, M.; Tamaura, Y. XRD and Mössbauer Studies on Oxygen-Deficient Ni(II)-Bearing Ferrite with a High Reactivity for CO_2 Decomposition to Carbon. *J. Solid State Chem.* **1995**, *120*, 64–69. [CrossRef]
246. Lin, K.S.; Adhikari, A.K.; Tsai, Z.Y.; Chen, Y.P.; Chien, T.T.; Tsai, H.B. Synthesis and characterization of nickel ferrite nanocatalysts for CO_2 decomposition. *Catal. Today* **2011**, *174*, 88–96. [CrossRef]
247. Tabata, M.; Akanuma, K.; Togawa, T.; Tsuji, M.; Tamaura, Y. Mössbauer study of oxygen-deficient Zn^{II}-bearing ferrites ($Zn_xFe_{3-x}O_{4-\delta}$, $0 \leq x \leq 1$) and their reactivity toward CO_2 decomposition to carbon. *J. Chem. Soc. Faraday Trans.* **1994**, *90*, 1171–1175. [CrossRef]
248. Sarangi, P.P.; Vadera, S.R.; Patra, M.K.; Ghosh, N.N. Synthesis and characterization of pure single phase Ni-Zn ferrite nanopowders by oxalate based precursor method. *Powder Technol.* **2010**, *203*, 348–353. [CrossRef]
249. Shin, H.C.; Choi, S.C.; Jung, K.D.; Han, S.H. Mechanism of M Ferrites (M = Cu and Ni) in the CO_2 decomposition reaction. *Chem. Mater.* **2001**, *13*, 1238–1242. [CrossRef]
250. Nordhei, C.; Mathisen, K.; Safonova, O.; van Beek, W.; Nicholson, D.G. Decomposition of Carbon Dioxide at 500 °C over Reduced Iron, Cobalt, Nickel, and Zinc Ferrites: A Combined XANES−XRD Study. *J. Phys. Chem. C* **2009**, *113*, 19568–19577. [CrossRef]
251. Nordhei, C.; Mathisen, K.; Bezverkhyy, I.; Nicholson, D. Decomposition of Carbon Dioxide over the Putative Cubic Spinel Nanophase Cobalt, Nickel, and Zinc Ferrites. *J. Phys. Chem. C* **2008**, *112*, 6531–6537. [CrossRef]
252. Wang, G.; Xu, S.; Jiang, L.; Wang, C. Nickel supported on iron-bearing olivine for CO_2 methanation. *Int. J. Hydrogen Energy* **2016**, *41*, 12910–12919. [CrossRef]
253. Swierczynski, D.; Courson, C.; Bedel, L.; Kiennemann, A.; Guille, J. Characterization of Ni-Fe/MgO/Olivine catalyst for fluidized bed steam gasification of biomass. *Chem. Mater.* **2006**, *18*, 4025–4032. [CrossRef]
254. Yang, X.; Xu, S.; Xu, H.; Liu, X.; Liu, C. Nickel supported on modified olivine catalyst for steam reforming of biomass gasification tar. *Catal. Commun.* **2010**, *11*, 383–386. [CrossRef]
255. Lu, H.; Yang, X.; Gao, G.; Wang, J.; Han, C.; Liang, X.; Li, C.; Li, Y.; Zhang, W.; Chen, X. Metal (Fe, Co, Ce or La) doped nickle catalyst supported on ZrO_2 modified mesoporous clays for CO and CO_2 methanation. *Fuel* **2016**, *183*, 335–344. [CrossRef]
256. Pandey, D.; Deo, G. Effect of support on the catalytic activity of Ni-Fe catalysts for CO_2 methanation reaction. *J. Ind. Eng. Chem.* **2016**, *33*, 99–107. [CrossRef]
257. Project Homepage—HELMETH. Available online: http://www.helmeth.eu/index.php/project (accessed on 16 December 2016).
258. Project Homepage—BioCat Project, Electrochaea. Available online: http://www.electrochaea.com/technology/ (accessed on 16 December 2016).
259. Kristjanpoller, F.; Crespo, A.; Barbera, L.; Viveros, P. Biomethanation plant assessment based on reliability impact on operational effectiveness. *Renew. Energy* **2017**, *101*, 301–310. [CrossRef]